Symmetry principles in the nuclear magnetic resonance of spinning solids: Heteronuclear recoupling by generalized Hartmann–Hahn sequences

Andreas Brinkmann and Malcolm H. Levitt[a)]
Division of Physical Chemistry, Arrhenius Laboratory, Stockholm University, S-106 91 Stockholm, Sweden

(Received 18 December 2000; accepted 12 April 2001)

General symmetry principles for rotor-synchronized pulse sequences in magic-angle spinning solid-state nuclear magnetic resonance are presented. The theory of symmetry-based pulse sequences using π pulse elements is presented for the first time. The symmetry theory is extended to the case of generalized Hartmann–Hahn sequences, in which rotor-synchronized rf irradiation is applied simultaneously to two isotopic spin species. The symmetry principles lead to heteronuclear selection rules. The symmetry theory is used to design pulse sequences which implement heteronuclear dipolar recoupling at the same time as decoupling homonuclear spin–spin interactions, and which also suppress chemical shift anisotropies. A number of specific pulse sequences based on these principles are listed. Experimental demonstrations are given of heteronuclear two-dimensional correlation spectroscopy, heteronuclear multiple-quantum spectroscopy, and the estimation of internuclear dipolar couplings. © *2001 American Institute of Physics.* [DOI: 10.1063/1.1377031]

I. INTRODUCTION

The determination of molecular structural parameters by solid-state nuclear magnetic resonance (NMR) has recently made much progress, with the successful development of methods for the accurate determination of internuclear distances[1–19] and interbond angles.[20–30] Many of these methods are compatible with magic-angle spinning (MAS),[31,32] in which the sample is rapidly rotated about an axis at the ''magic angle'' $\tan^{-1}\sqrt{2}$ with respect to the static magnetic field in order to achieve good spectral resolution and signal strength.

Although MAS is an essential component of many realistic applications of solid-state NMR, it has the disadvantage of strongly attenuating the effect of geometrically informative spin interactions, such as the direct magnetic dipole–dipole couplings between neighboring nuclear spins. As a result, the techniques for geometry determination often employ *recoupling* pulse schemes, in which resonant radio-frequency (rf) fields are applied to the nuclear spins, in order to suspend the averaging effect of the magic-angle rotation over a defined time interval. This makes it possible to exploit the recoupled spin interactions for the determination of molecular geometry, without sacrificing the good sensitivity and resolution provided by MAS.

There are many different types of recoupling pulse sequences, depending upon the targeted spin interaction.[33,34] For example, there exists a wide range of pulse sequences for recoupling the direct dipole–dipole interactions between spins of the same isotopic type. These are called *homonuclear* recoupling methods. This article focuses on the methodology of *heteronuclear* recoupling, in which the magnetic dipole–dipole interactions between unlike spins are recoupled.

Heteronuclear recoupling methods face a number of methodological challenges associated with the type of nuclear spin system involved and with instrumental limitations. For example, it is often desirable to recouple the *hetero*nuclear dipole–dipole interactions, without simultaneously recoupling the *homo*nuclear dipole–dipole interactions. In addition, it is often desirable that the evolution of the nuclear spin system is insensitive to chemical shift interactions, both isotropic and anisotropic. In a nonoriented sample such as a powder, there are further complications, since the recoupling effect depends in general on the molecular orientation. In most cases it is desirable that the orientation dependence of the recoupling be as weak as possible, so as to obtain good overall efficiency in a orientationally disordered sample such as a powder. The recoupling methodology should also be robust with respect to deviations in the amplitude of the applied rf field. In addition, it is sometimes necessary that the pulse sequences are feasible at very high magic-angle spinning frequencies.

The Hartmann–Hahn (HH) method is the archetypical heteronuclear solid-state NMR method. This early scheme involves the simultaneous application of two unmodulated rf fields, each resonant with a different spin species, and with amplitudes chosen so that the two nutation frequencies match exactly.[35] HH matching allows a transfer of spin polarization between different spin isotopes, through the heteronuclear dipolar interaction. Hartmann–Hahn cross polarization (HH-CP) is widely employed in solid-state NMR for the enhancement of signals from nuclei with low gyromagnetic ratios and is an essential component of high-resolution NMR in solids.[36] The Hartmann–Hahn method was originally developed for static solids but may be used in MAS NMR if the rf field amplitudes are adjusted so that the two nutation frequencies differ by a small integer multiple of the spinning frequency. This is called a HH sideband

a)Electronic mail: mhl@physc.su.se

TABLE I. The qualitative properties of selected heteronuclear recoupling sequences. A check mark means that the corresponding sequence has the indicated property in a first order theoretical description. A cross means it does not have this property.

Sequence	Ref.	γ encoding of *SK*-DD	*KK*-DD decoupling	*K*-CSA decoupling	*K*-CSA insensitivity	*K*-offset insensitivity	rf field compensation	rf field requirements
Single-channel sequences (irradiation at *K*-spin Larmor frequency)								
R^3	1, 2	√	×	×	×	(√)	×	low
SPI-R^3	25	×	×	×	√	(√)	√	low
REDOR	3, 4	×	×	×	√	√	√	high
C-REDOR	48	×	√	×	√	√	√	low/moderate
T-MREV	28, 29	√	(√)	×	×	√	√	moderate
$R18_1^7$	17	√	√	×	×	√	√	moderate
Two-channel sequences (irradiation at *K*- and *S*-spin Larmor frequencies)								
HH-CP	35, 36	√	×	√	√	√	×	moderate
LG-HH-CP	18	√	(√)	√	√	×	×	moderate
two-channel symmetry-based sequences	this paper	√	√	√	√	√	√	moderate

condition.[37] The sensitivity of the HH method to experimental imperfections may be reduced by sweeping the amplitude of one of the radio-frequency fields so as to pass through the appropriate matching condition.[38,76–78]

In its original version, the Hartmann–Hahn method does not decouple the homonuclear interactions. In many cases, this makes the method unsuitable for extracting accurate molecular structural information. In static solids, homonuclear decoupling may be combined with HH-CP by setting one or both of the rf fields off resonance, so as to satisfy the Lee–Goldburg condition.[39,92] A sideband version of Lee–Goldburg Hartmann–Hahn cross polarization (LG-HH-CP) has been applied to MAS solids, allowing the determination of distances between nuclei of different types, even in the presence of strong homonuclear couplings.[18,19]

A different group of heteronuclear recoupling methods involves the application of radio-frequency fields to only one of the spin species. This type of heteronuclear recoupling was first achieved in MAS NMR by setting the amplitude of the rf field so that the nutation frequency matches a small integer multiple of the spinning frequency. This is called rotary resonance recoupling (R^3).[1,2] It was also suggested that the unmodulated rf field could be replaced by discrete π pulses every half rotor period.[2,3] Experiments of this kind were first performed by Gullion *et al.*, and form the basis of the highly successful REDOR (Rotational Echo Double Resonance) method.[3,4] Numerous applications and extensions of REDOR have appeared.[40–43]

The original version of REDOR employs very strong π pulses, which are assumed to be very short compared to the sample rotation period. This condition is hard to meet at high MAS spinning frequencies. Modulated versions of R^3 were suggested for use at high MAS frequencies.[44,45] It was demonstrated that in some circumstances REDOR itself functions quite satisfactorily even under fast MAS conditions.[46]

Table I summarizes a variety of existing heteronuclear recoupling sequences and displays their qualitative properties. This table assumes that there are two spin species, called here *S* and *K*. In the case of single-channel pulse sequences, the rf irradiation is assumed to be resonant with the *K* spins. All of the pulse sequences recouple the first-order heteronuclear direct dipolar interaction (abbreviated *SK*-DD).

The third column in the table indicates whether the recoupled *SK* dipolar interaction is ''γ encoded.''[10] This property is explained in more detail below. Briefly, γ-encoded pulse sequences have a lower orientation dependence than non-γ-encoded pulse sequences, and as a result generally function better in a powder sample. The fourth column indicates whether the homonuclear dipole–dipole interactions between *K* spins are decoupled. Generally speaking, homonuclear decoupling of *K* spins is also a desirable property, since it greatly simplifies the spin dynamics and reduces the approximations that must be made when analyzing the experimental results. The fifth column indicates whether the pulse sequence effectively removes the chemical shift anisotropy (CSA) interactions of the *K* spins in the first-order average Hamiltonian.[47] The sixth column indicates whether the evolution of the *S* spins is insensitive to the CSA of the *K* spins. This is a slightly weaker condition than that given in the fifth column, since in some circumstances, commutation properties cause the evolution of the relevant *S*-spin coherences to be insensitive to the *K*-spin CSA, even if that CSA interaction is not fully decoupled. The seventh column indicates whether the sequence is compensated for isotropic chemical shift or resonance offsets of the *K* spins. The eighth column indicates whether the sequence is compensated for rf field amplitude variations. The ninth column indicates the rough rf field requirements of the sequence. In all cases, these ''judgments'' are based on first-order average Hamiltonian theory.[47] They should be regarded as a provisional basis for discussion, rather than a definitive assessment.

With these reservations in mind, all existing sequences display a mixture of positive and negative qualities. For example, the REDOR sequence[3,4] displays an array of robust features with respect to the *K*-spin interactions. The sequence is well-compensated for rf field errors and *K*-spin chemical shifts, both isotropic and anisotropic. However, it has its negative side too. REDOR is not γ encoded, which implies

that the signal modulations due to the heteronuclear *SK* interactions are relatively weak in powder samples. In addition, the homonuclear dipolar interactions between *K* spins are also recoupled. This can cause trouble when the sequence is applied to strongly interacting spins. REDOR also recouples the *K*-spin CSA interactions, but this turns out not to be a problem in most applications, since the relevant recoupled interactions commute (see the contrasting marks in columns 6 and 7). REDOR was originally designed for work at low spinning frequencies and has high rf field requirements. However, recent results indicate that REDOR may in fact be usable even at high MAS frequencies.[46]

A recent variant of REDOR, called C-REDOR,[48] achieves homonuclear decoupling (see Sec. IV below).

As a second example, consider the sideband Lee–Goldburg Hartmann–Hahn method.[18] In this case the recoupled heteronuclear interactions are γ encoded, indicating favorable performance in a powder. The sideband LG-HH method also strongly attenuates the *K*-spin CSA interactions. However, the decoupling of the homonuclear *K*-spin DD interactions is expected to be imperfect. The original Lee–Goldburg scheme for homonuclear decoupling[39] is known to be relatively poor and has long been superseded by more accurate schemes in the case of high-resolution proton spectroscopy.[49–54] In addition, the use of LG decoupling is well-established for static samples, but its performance may be degraded in rapidly rotating samples, due to interference effects between the rf pulse sequence and the MAS rotation. For this reason, we have only given the LG-HH method a bracketed tick mark in column 4. In addition, the LG method is sensitive to *K*-spin chemical shifts and rf field amplitude errors.

The table shows that the REDOR and LG-HH methods are roughly complementary in their strengths and weaknesses.

A different approach to pulse sequence design exploits symmetry principles for rotor-synchronized rf fields in MAS NMR.[17,55] These principles allow the recoupling and decoupling properties of a wide range of pulse sequences to be assessed, at least to a first approximation, by evaluating a set of simple integer inequalities. The results of these inequalities may be deduced by a diagrammatic technique without detailed calculation. In addition, it is possible to identify sets of pulse sequence symmetries that lead to the recoupling properties of interest, at least in a first approximation.

Briefly, the symmetry theory may be applied to two broad pulse sequence classes, denoted in general CN_n^ν and RN_n^ν. The meaning of these symbols is explained in detail below. The numbers *N*, *n*, and ν are small integers, called the symmetry numbers of the pulse sequence.

So far, the symmetry principles have only been presented for the case of rf irradiation on a single rf channel. These single-channel symmetry principles have led to a large selection of promising pulse sequences for heteronuclear decoupling,[17,55] double-quantum homonuclear recoupling,[11,14,17,56] zero-quantum homonuclear recoupling,[17] and selection of homonuclear *J*-couplings.[17,57,58] In addition, the symmetry principles provide insight into a variety of existing methods, such as REDOR,[3,4] RFDR[59] and TPPM.[60]

The single-channel symmetry principles have also been applied to the problem of heteronuclear recoupling in the presence of strong homonuclear couplings. For example, a single-channel heteronuclear recoupling sequence with the symmetry $R18_1^7$ was demonstrated.[17] The qualitative properties of this sequence are also given in Table I. As may be seen, the sequence has a number of desirable features, but retains an undesirable sensitivity to the CSA of the irradiated *K* spins. It is difficult to accomplish γ-encoded heteronuclear decoupling with rf irradiation on a single rf channel while simultaneously removing the sensitivity of the sequence to the *K*-spin CSA. The symmetry theory alone does not lead to solutions of this kind.

In this paper the symmetry principles are extended to the case of a heteronuclear spin system exposed to simultaneous resonant irradiation on two rf channels. Such sequences may be regarded as *generalized Hartmann–Hahn methods*. We show that it is possible to design pulse sequences that possess all of the desirable features in Table I, at least on the level of first-order average Hamiltonian theory. As shown below, the extended symmetry theory leads to a large number of possible solutions. We show experimental results for some of the more promising pulse sequences.

The rest of this paper is organized as follows. In Sec. II we present the symmetry theory for single-channel CN_n^ν and RN_n^ν sequences. Much of this work has not been presented explicitly before. In Sec. III these principles are generalized to the case of dual synchronized CN_n^ν and RN_n^ν sequences. In Sec. IV we identify a list of candidate symmetries for the task of heteronuclear recoupling and present some specific pulse sequences based on these principles. In Sec. V we show some experimental results, including applications to heteronuclear two-dimensional (2D) correlation spectroscopy, heteronuclear multiple-quantum NMR, and heteronuclear distance estimations. The applications and limitations of the new pulse sequences are discussed.

II. SINGLE-CHANNEL ROTOR-SYNCHRONIZED PULSE SEQUENCES

We first consider the case of a rotor-synchronized pulse sequence applied to one rf channel. The symmetry rules for this situation have been described before,[17,55] but the detailed theory has not yet been presented for the case of RN_n^ν sequences. The discussion here will establish the notation and lay the groundwork for the two-channel case.

A. Euler angles of the rf rotations

Consider a system of coupled *S* spins, subjected to mechanical sample rotation at a fixed frequency ω_r about a fixed axis. The spin Hamiltonian in the presence of a rf pulse sequence is given by

$$H(t) = H_{\mathrm{rf}}(t) + H_{\mathrm{int}}(t), \tag{1}$$

where the internal spin Hamiltonian $H_{\mathrm{int}}(t)$ is time dependent because of the sample rotation, while the rf spin Hamiltonian $H_{\mathrm{rf}}(t)$ is time dependent because of the modulation of the rf fields. The rf propagator from a time point t_a to a time point t_b is denoted $U_{\mathrm{rf}}(t_b, t_a)$, and solves the equations

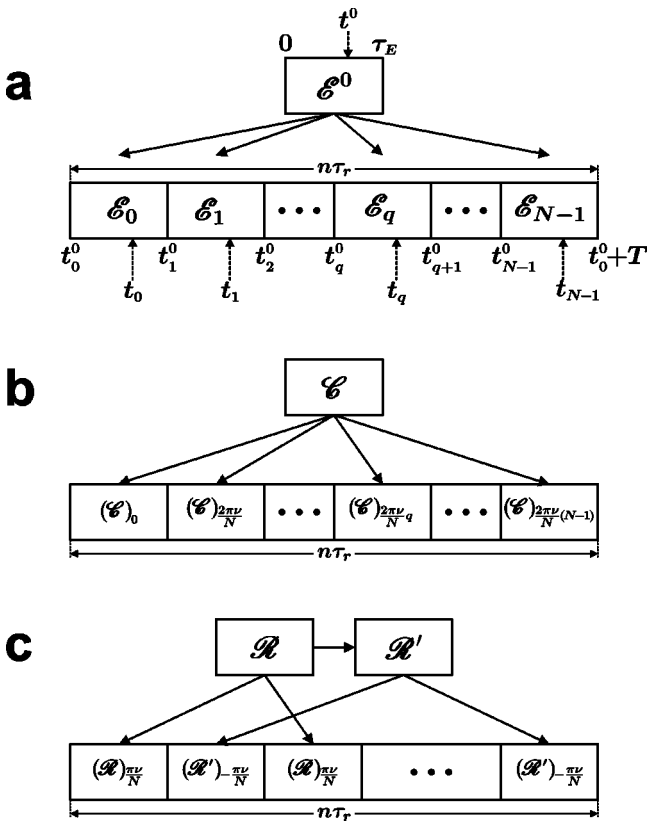

FIG. 1. Definitions of rotor synchronized pulse sequences. (a) Pulse sequence built up of N elements $\mathscr{E}_q$, where $q=0,1,...,N-1$. The whole sequence spans exactly n rotational periods. A selection of time points is indicated. (b) One way to implement a CN_n^ν sequence. The basic element $\mathscr{C}$ is given by a rf cycle. The CN_n^ν sequence is composed of N phase-shifted cycles. (c) One way to implement a RN_n^ν sequence. The basic element $\mathscr{R}$ implements a π rotation about the x axis. The element $\mathscr{R}'$ is obtained from $\mathscr{R}$ by changing the sign of all phases. The RN_n^ν sequence is composed of $N/2$ phase-alternating $\mathscr{R}\mathscr{R}'$ pairs.

$$\frac{d}{dt}U_{\rm rf}(t,t_a)=-iH_{\rm rf}(t)U_{\rm rf}(t,t_a), \tag{2}$$

$$U_{\rm rf}(t_a,t_a)=1. \tag{3}$$

Suppose that the rf pulse sequence is initiated at time point t_0^0 [see Fig. 1(a)]. The rf propagator from time point t_0^0 up to an arbitrary time point t may be expressed in terms of three time dependent Euler angles $\Omega(t)=\{\alpha(t),\beta(t),\gamma(t)\}$, describing the rotation of the spins induced by the rf field:

$$U_{\rm rf}(t,t_0^0)=R_z[\alpha(t)]R_y[\beta(t)]R_z[\gamma(t)]. \tag{4}$$

Here $R_\chi=\exp\{-i\phi S_\chi\}$ is the operator for a rotation of spins S through the angle ϕ around the axis $\chi=(x,y,z)$ in the rotating frame. If the rf fields are applied at the Larmor frequency of species S, the operator S_χ is given by

$$S_\chi=\sum_j S_{j\chi}, \tag{5}$$

where the sum is taken over all S spins.

In general, the rf propagator for any rf pulse sequence may be written in terms of the Euler angles as in Eq. (4). However, in general, the link between the Euler angles and the rf irradiation parameters (pulse flip angles and phases) is sometimes not obvious.

B. Notation for time points

Consider a general rotor-synchronized pulse sequence as shown in Fig. 1(a). The pulse sequence is built of N elements, denoted $\mathscr{E}_q$, where $q=0,...,N-1$. The whole sequence spans exactly n rotational periods. Each element $\mathscr{E}_q$ has the same duration $\tau_E=n\tau_r/N$, where $\tau_r=2\pi/\omega_r$. The duration of the entire sequence is denoted $T=N\tau_E=n\tau_r$.

Figure 1(a) defines the convention used for denoting time points in this paper. The time point t_q^0 defines the instant at which the element $\mathscr{E}_q$ starts. The notation t_q defines an arbitrary time point in the interval $[t_q^0,t_{q+1}^0[$, i.e., $t_q^0\leqslant t_q<t_{q+1}^0$. The time points are related through $t_q=t_0+q\tau_E$. The notation t_0 refers to a time point in the interval $[t_0^0,t_1^0[$, i.e., within the first element $\mathscr{E}_0$.

We use the notation S_q to refer to the rf propagator up to a general time point t_q within an element $\mathscr{E}_q$, starting from the beginning of that element. The notation A_q refers to the rf propagator up to a general time point t_q within an element $\mathscr{E}_q$, accumulated over the whole pulse sequence. The notation E_q refers to an rf propagator of one complete element $\mathscr{E}_q$:

$$S_q=U_{\rm rf}(t_q,t_q^0), \tag{6}$$

$$A_q=U_{\rm rf}(t_q,t_0^0), \tag{7}$$

$$E_q=U_{\rm rf}(t_{q+1}^0,t_q^0). \tag{8}$$

These propagators are related through

$$A_q=S_qE_{q-1}E_{q-2}\cdots E_0. \tag{9}$$

The Euler angles $\Omega_q=\{\alpha_q,\beta_q,\gamma_q\}=\{\alpha(t_q),\beta(t_q),\gamma(t_q)\}$ refer to the accumulated rf rotations up to a general time point t_q within the element $\mathscr{E}_q$:

$$A_q=R_z(\alpha_q)R_y(\beta_q)R_z(\gamma_q). \tag{10}$$

C. The basic element

In the sequences to be described, all the elements $\mathscr{E}_q$ are derived in a specified way from a given pulse sequence of duration $\tau_E=n\tau_r/N$, known as the basic element, and denoted here $\mathscr{E}^0$. The properties of $\mathscr{E}^0$ depend on the symmetry class of the pulse sequence and will be described below.

In general the basic element $\mathscr{E}^0$ is never actually applied to the spin system, only the derived elements $\mathscr{E}_q$ have that honor. Nevertheless, it is convenient to denote the rf propagators of the basic element $\mathscr{E}^0$ by using the superscript ''0.'' Figure 1(a) defines the convention used for denoting time points inside the basic element $\mathscr{E}^0$. The basic element starts at time point 0 and finishes at time point τ_E. The notation t^0 defines an arbitrary time point inside the interval $[0,\tau_E[$, i.e., $0\leqslant t^0<\tau_E$. The time point t^0 inside the basic element $\mathscr{E}^0$ and the time point t_0 inside the first element $\mathscr{E}_0$ are related through

$$t^0=t_0-t_0^0. \tag{11}$$

The rf field Hamiltonian of sequence $\mathscr{E}^0$ is denoted $H^0_{\mathrm{rf}}(t)$ and the rf propagator under the basic element $\mathscr{E}^0$ is denoted $U^0_{\mathrm{rf}}(t^0,0)$. The accumulated propagator under $\mathscr{E}^0$ at time point t^0 and the corresponding Euler angles are

$$S^0=A^0=R_z(\alpha^0)R_y(\beta^0)R_z(\gamma^0)=U^0_{\mathrm{rf}}(t^0,0). \tag{12}$$

The propagator under the entire basic element $\mathscr{E}^0$ is denoted

$$E^0=U^0_{\mathrm{rf}}(\tau_E,0). \tag{13}$$

In general E^0 (the propagator under the basic element) is not equal to E_0 (the propagator under the first element in the pulse sequence).

D. Definition and implementation of CN^{ν}_{n} sequences

A general CN^{ν}_{n} sequence on the S spins is defined by the following time-symmetry relationships for the Euler angles of the rf propagator at time points t_q:

$$\beta_q=\beta_0, \quad \gamma_q=\gamma_0-\frac{2\pi\nu}{N}q. \tag{14}$$

Here $q=0,1,...,N-1$ and the duration of each element is $\tau_E=n\tau_r/N$.

Equation (14) defines the symmetry class of the CN^{ν}_{n} sequences, through the three symmetry numbers N, n, and ν. The Euler angles β_q and γ_q of the rf propagator at time points separated by a multiple of τ_E are connected to each other by a simple symmetry transformation. Note that the CN^{ν}_{n} symmetry implies no restrictions on the angles α_q.

Figure 1(b) shows one possible construction scheme for CN^{ν}_{n} sequences. The method starts by choosing a basic element $\mathscr{E}^0$, which has the following propagator,

$$E^0=R_x(Z_g\pi), \tag{15}$$

where Z_g is an even integer (g stands for ''gerade''). This implies that the basic element returns spins to their initial states (disregarding a possible sign change), if all interactions other than that with the rf field are ignored. The basic element is therefore a cycle in the sense of Haeberlen and Waugh[47] and will henceforth be denoted $\mathscr{C}$. Some examples of $\mathscr{C}$ sequences are given below.

As shown in Fig. 1(b), a CN^{ν}_{n} sequence may be constructed by concatenating N cyclic elements, each of which is phase shifted by $2\pi/N$ with respect to the preceding element, i.e.,

$$\mathscr{E}_q=(\mathscr{C})_{2\pi\nu q/N}. \tag{16}$$

This implies that the first element $\mathscr{E}_0$ of the CN^{ν}_{n} sequence is the same as the basic element $\mathscr{C}$, and hence that $(\alpha_0,\beta_0,\gamma_0)=(\alpha^0,\beta^0,\gamma^0)$. In Appendix A we prove that this procedure generates a CN^{ν}_{n} sequence conforming to Eq. (14).

The symmetry numbers n and ν are called space and spin winding numbers, respectively, since they define the helical modulations of the two parts of the Hamiltonian, as discussed in Ref. 56.

The choice of $\mathscr{C}$ is free within the constraints of Eq. (15). For example, the basic rf cycle $\mathscr{C}$ could be a simple 360° pulse around the x axis as in the SC14 sequence[56] ($\mathscr{C}=360_0$), or a composite 360° pulse, as in the original C7 sequence[11] ($\mathscr{C}=360_0360_{180}$), or in the POST-C7[13] and the SPC-5 sequences[14] ($\mathscr{C}=90_0360_{180}270_0$). Here the standard notation for rf pulse sequences is used: ξ_ϕ, where ξ is the flip angle (nutation frequency multiplied by the pulse duration) and ϕ is the rf phase, taking into account the sign of the gyromagnetic ratio.[61,62] The flip angles and the phases are written in degrees.

There are also other ways of constructing CN^{ν}_{n} sequences which satisfy Eq. (14) (see below).

E. Definition and implementation of RN^{ν}_{n} sequences

A general RN^{ν}_{n} sequence is defined by the following time-symmetry relationships for the Euler angles of the rf propagators:

$$\beta_q=\beta_0+q\pi, \quad \gamma_q=\gamma_0-\frac{2\pi\nu}{N}q, \tag{17}$$

where $q=0,1,...,N-1$. The duration of each element $\mathscr{E}_q$ is $\tau_E=n\tau_r/N$, and N, n, and ν are integers, called the symmetry numbers of the pulse sequence. There are no restrictions on the Euler angle α_q.

Figure 1(c) shows one possible construction scheme for a RN^{ν}_{n} sequence. The method starts by choosing a basic element of duration τ_E. In this case, the rf propagator of the basic element has the property

$$E^0=R_x(Z_u\pi), \tag{18}$$

where Z_u is an odd integer (u stands for ''ungerade''). This implies that the basic element rotates the spins by an odd multiple of π about the x axis in the rotating frame. In this case the basic element is donated $\mathscr{R}$, to confirm with standard notation in heteronuclear decoupling theory.[63] The basic element $\mathscr{R}$ may therefore be a single $(\pi)_x$ pulse, or a composite pulse with the same overall rotation. In general, the basic element $\mathscr{R}$ may contain rf pulses of any possible phase, but the overall rotation operator must obey Eq. (18).

The construction principle for RN^{ν}_{n} sequences continues by deriving a second basic element, denoted $\mathscr{R}'$, which is related to $\mathscr{R}$ by changing the sign of all rf phases. The rf propagator under $\mathscr{R}'$ may be derived from that under $\mathscr{R}$ by a π rotation about the x axis:

$$E^{0\prime}=R_x(\pi)E^0R_x(\pi)^{\dagger}. \tag{19}$$

If the basic element contains amplitude modulated rf fields (i.e., all phase changes are multiples of π), then $\mathscr{R}'$ and $\mathscr{R}$ are identical. In all other cases $\mathscr{R}'$ and $\mathscr{R}$ are different sequences. For example, if $\mathscr{R}=90_{90}180_090_{90}$, then $\mathscr{R}'=90_{-90}180_090_{-90}$.

A RN^{ν}_{n} sequence may be constructed by concatenating $N/2$ phase-shifted $\mathscr{R}\mathscr{R}'$ pairs as follows:

$$\mathscr{E}_q=\begin{cases}(\mathscr{R})_{\pi\nu/N} & \text{for } q=\text{even}\\ (\mathscr{R}')_{-\pi\nu/N} & \text{for } q=\text{odd}.\end{cases} \tag{20}$$

Note that the first element $\mathscr{E}_0$ of a RN^{ν}_{n} sequence is not equal to the basic element $\mathscr{R}$. The procedure is illustrated in Fig. 1(c). In Appendix A we prove that this procedure generates a RN^{ν}_{n} sequence conforming to Eq. (17).

TABLE II. Homonuclear spin interactions in a solid rotating at the magic angle with respect to the external magnetic field, and their properties with respect to spatial and spin rotations. The spatial components with $m=0$ disappear for exact magic-angle spinning, in the case $l=2$.

Interaction	Space rank l	Space component m	Spin rank λ	Spin component μ
isotropic chemical shift	0	0	1	−1, 0, 1
CSA	2	−2, −1, 1, 2	1	−1, 0, 1
homonuclear isotropic J coupling	0	0	0	0
homonuclear dipolar coupling	2	−2, −1, 1,2	2	−2,−1,0, 1, 2

From the definition of $\mathrm{R}N_n^\nu$ symmetry [Eq. (17)], any $\mathrm{R}N_n^\nu$ sequence is also a $\mathrm{C}(N/2)_n^\nu$ sequence, even though its construction principles are quite different. This implies that $\mathrm{R}N_n^\nu$ symmetry is a stronger version of $\mathrm{C}(N/2)_n^\nu$ symmetry. This property is reflected in the more restrictive selection rules for $\mathrm{R}N_n^\nu$ sequences compared to $\mathrm{C}N_n^\nu$ sequences (see below).

F. Spin interactions

In a system of coupled spins S the internal spin Hamiltonian in Eq. (1) at time point t may be written

$$H_{\mathrm{int}}(t)=\sum_{\Lambda,l,m,\lambda} H_{lm\lambda 0}^{\Lambda}(t), \tag{21}$$

where the symbol Λ represents the type of interaction (chemical shift, spin–spin coupling) and also the indices of the spins involved in the interaction.

The quantum numbers l, m, and λ indicate the symmetry of the term with respect to rotations of the spin polarizations and with respect to spatial rotations of the sample. In general the term $H_{lm\lambda\mu}^{\Lambda}(t)$ transforms as an irreducible spherical tensor of rank l for spatial rotations and rank λ for spin rotations. The components indices m and μ take values $m=-l,-l+1,...,l$ for space and $\mu=-\lambda,-\lambda+1,...,\lambda$ for spin. Table II contains a list of interactions in a homonuclear spin system, the corresponding values for the ranks l and λ, and the possible components m and μ under magic-angle rotation of the sample. In the high-field approximation the internal Hamiltonian contains only elements with $\mu=0$. Terms with $\mu\neq 0$ are generated by the applied rf field (see below). Because of the sample rotation, the term $H_{lm\lambda 0}^{\Lambda}(t)$ is periodically modulated:

$$H_{lm\lambda 0}^{\Lambda}(t)=\omega_{lm}^{\Lambda}\exp\{im\omega_r t\}T_{\lambda 0}^{\Lambda} \tag{22}$$

with the complex amplitudes

$$\omega_{lm}^{\Lambda}=[A_{lm}^{\Lambda}]^R d_{m0}^{l}(\beta_{RL})\exp\{-im\alpha_{RL}^{0}\}, \tag{23}$$

where α_{RL}^{0} denotes the initial rotor position and β_{RL} defines the angle between the rotor axis and the static magnetic field direction ($\beta_{RL}=\arctan\sqrt{2}$ for magic angle spinning). d_{m0}^{l} is a reduced Wigner element. Note that $d_{00}^{2}(\beta_{RL})=0$ in the case of exact MAS. $T_{\lambda\mu}^{\Lambda}$ is the μth component of the spin tensor of rank λ from interaction Λ.

$[A_{lm}^{\Lambda}]^R$ defines the rotational properties of the spin interaction under mechanical rotation of the sample, keeping the external magnetic field fixed. The relevant tensor component of rank l is obtained in the rotor fixed frame by transforming it from the principal axis system as follows:

$$[A_{lm}^{\Lambda}]^R=\sum_{m'',m'}[A_{lm''}^{\Lambda}]^P D_{m''m'}^{l}(\Omega_{PM}^{\Lambda})D_{m'm}^{l}(\Omega_{MR}). \tag{24}$$

The Euler angles $\Omega_{PM}^{\Lambda}=\{\alpha_{PM}^{\Lambda},\beta_{PM}^{\Lambda},\gamma_{PM}^{\Lambda}\}$ describe the relative orientation of the principal axis frame of the interaction Λ and a molecule-fixed frame, and depend on the molecular and electronic structure. The Euler angles $\Omega_{MR}=\{\alpha_{MR},\beta_{MR},\gamma_{MR}\}$ relate the molecular frame to a frame fixed on the rotor, and are random variables in a powder.

From Eq. (22) and the definition $t_q=t_0+q\tau_E$, the periodic symmetry of the laboratory frame spin interaction terms for the rotor-synchronized pulse sequence shown in Fig. 1(a) may be expressed

$$H_{lm\lambda 0}^{\Lambda}(t_q)=H_{lm\lambda 0}^{\Lambda}(t_0)\exp\left\{i\frac{2\pi m}{N}q\right\}. \tag{25}$$

G. Interaction frame symmetry

Average Hamiltonian theory[47] requires a transformation of the spin interaction terms into the interaction frame of the rf field. The interaction frame Hamiltonian at time point t_q may in general be written

$$\tilde{H}(t_q)=\sum_{\Lambda,l,m,\lambda,\mu}\tilde{H}_{lm\lambda\mu}^{\Lambda}(t_q), \tag{26}$$

where

$$\tilde{H}_{lm\lambda\mu}^{\Lambda}(t_q)=\frac{\mathrm{Tr}\{T_{\lambda\mu}^{\Lambda\dagger}A_q^{\dagger}H_{lm\lambda 0}^{\Lambda}(t_q)A_q\}}{\mathrm{Tr}\{T_{\lambda\mu}^{\Lambda\dagger}T_{\lambda\mu}^{\Lambda}\}}T_{\lambda\mu}^{\Lambda}. \tag{27}$$

In this case μ takes all possible values $\mu=-\lambda,-\lambda+1,...,\lambda$. The rotation properties of spherical tensor operators[64]

$$R_z(-\gamma)R_y(-\beta)R_z(-\alpha)T_{\lambda 0}^{\Lambda}R_z(\alpha)R_y(\beta)R_z(\gamma)$$

$$=\sum_{\mu} d_{\mu 0}^{\lambda}(-\beta)\exp\{i\mu\gamma\}T_{\lambda\mu}^{\Lambda} \tag{28}$$

lead to the following form of the interaction frame terms:

$$\tilde{H}_{lm\lambda\mu}^{\Lambda}(t_q)=d_{\mu 0}^{\lambda}(-\beta_q)\omega_{lm}^{\Lambda}\exp\{i\mu\gamma_q+im\omega_r t_q\}T_{\lambda\mu}^{\Lambda}. \tag{29}$$

The symmetry of the terms depend on the symmetry of the pulse sequence.

(i) $\mathrm{C}N_n^\nu$ *sequences*: Equations (14) and (29) may be used to show that the $\mathrm{C}N_n^\nu$ symmetry of the pulse sequence imposes the following periodic symmetry on the interaction frame terms:

$$\tilde{H}_{lm\lambda\mu}^{\Lambda}(t_q)=\tilde{H}_{lm\lambda\mu}^{\Lambda}(t_0)\exp\left\{i\frac{2\pi q}{N}(mn-\mu\nu)\right\}. \tag{30}$$

(ii) $\mathrm{R}N_n^\nu$ *sequences*: Equations (17) and (29) lead to the following symmetry of the interaction frame terms:

$$\tilde{H}^{\Lambda}_{lm\lambda\mu}(t_q)=\tilde{H}^{\Lambda}_{im\lambda\mu}(t_0)\exp\left\{i\frac{2\pi q}{N}(mn-\mu\nu)\right\}d^{\lambda}_{\mu 0}(\pi q). \tag{31}$$

Since $d^{\lambda}_{\mu 0}(\pi q)=(-1)^{q\lambda}$, this symmetry may be written in the more convenient form

$$\tilde{H}^{\Lambda}_{lm\lambda\mu}(t_q)=\tilde{H}^{\Lambda}_{lm\lambda\mu}(t_0)\exp\left\{i\frac{2\pi q}{N}\left(mn-\mu\nu-\frac{\lambda N}{2}\right)\right\}. \tag{32}$$

The main difference between the two symmetries is that the spin rank λ appears in Eq. (32). This has major consequences.

H. Average Hamiltonian and selection rules

One may analyze the CN^{ν}_{n} and RN^{ν}_{n} sequences using the Magnus expansion[65] of the effective Hamiltonian in the interaction frame:

$$\bar{H}=\bar{H}^{(1)}+\bar{H}^{(2)}+\bar{H}^{(3)}+\cdots, \tag{33}$$

where the first two orders[65,66] are given by

$$\bar{H}^{(1)}=T^{-1}\int_{t_0^0}^{t_0^0+T}dt\tilde{H}(t), \tag{34}$$

$$\bar{H}^{(2)}=(2iT)^{-1}\int_{t_0^0}^{t_0^0+T}dt'\int_{t_0^0}^{t'}dt[\tilde{H}(t'),\tilde{H}(t)]. \tag{35}$$

The first order term is given by

$$\bar{H}^{(1)}=\sum_{\Lambda,l,m,\lambda,\mu}\bar{H}^{\Lambda}_{lm\lambda\mu}, \tag{36}$$

where

$$\bar{H}^{\Lambda}_{lm\lambda\mu}=T^{-1}\int_{t_0^0}^{t_0^0+T}dt\tilde{H}^{\Lambda}_{lm\lambda\mu}(t). \tag{37}$$

The second order term may be written in the following way:

$$\bar{H}^{(2)}=\sum_{\Lambda_2,\mathbf{2},\Lambda_1,\mathbf{1}}\bar{H}^{\Lambda_2\times\Lambda_1}_{\mathbf{2};\mathbf{1}}, \tag{38}$$

where the vectors **1** and **2** represent the sets of quantum numbers $(l_1,m_1,\lambda_1,\mu_1)$ and $(l_2,m_2,\lambda_2,\mu_2)$, respectively. The terms $\bar{H}^{\Lambda_2\times\Lambda_1}_{\mathbf{2};\mathbf{1}}$ are given by

$$\bar{H}^{\Lambda_2\times\Lambda_1}_{\mathbf{2};\mathbf{1}}=(2iT)^{-1}\int_{t_0^0}^{t_0^0+T}dt'\int_{t_0^0}^{t'}dt \times[\tilde{H}^{\Lambda_2}_{l_2m_2\lambda_2\mu_2}(t'),\tilde{H}^{\Lambda_1}_{l_1m_1\lambda_1\mu_1}(t)]. \tag{39}$$

The periodic symmetries given in Eqs. (30) and (32) lead to selection rules for these average Hamiltonians:

(i) CN^{ν}_{n} *sequences*: The following selection rules were derived in Ref. 55:

$$\bar{H}^{\Lambda}_{lm\lambda\mu}=0 \quad \text{if } mn-\mu\nu\neq NZ, \tag{40}$$

$$\bar{H}^{\Lambda_2\times\Lambda_1}_{\mathbf{2};\mathbf{1}}=0 \text{ if } \begin{cases} m_1n-\mu_1\nu\neq NZ, \\ \text{AND} \\ m_2n-\mu_2\nu\neq NZ \\ \text{AND} \\ (m_2+m_1)n-(\mu_2+\mu_1)\nu\neq NZ, \end{cases} \tag{41}$$

where Z is any integer.

(ii) RN^{ν}_{n} *sequences*: The selection rules are

$$\bar{H}^{\Lambda}_{lm\lambda\mu}=0 \quad \text{if } mn-\mu\nu\neq\frac{N}{2}Z_{\lambda}, \tag{42}$$

$$\bar{H}^{\Lambda_2\times\Lambda_1}_{\mathbf{2};\mathbf{1}}=0 \text{ if } \begin{cases} m_1n-\mu_1\nu\neq\dfrac{N}{2}Z_{\lambda_1} \\ \text{AND} \\ m_2n-\mu_2\nu\neq\dfrac{N}{2}Z_{\lambda_2} \\ \text{AND} \\ (m_2+m_1)n-(\mu_2+\mu_1)\nu\neq\dfrac{N}{2}Z_{\lambda_{2+\lambda_1}}, \end{cases} \tag{43}$$

where Z_{λ} indicates any integer with the same parity as λ.

Equation (42) may be deduced as follows. From Eq. (32) and the symmetry arguments given in the appendix of Ref. 55, we get

$$\bar{H}^{\Lambda}_{lm\lambda\mu}=0 \text{ if } mn-\mu\nu-\frac{\lambda N}{2}\neq NZ, \tag{44}$$

where Z is an integer. This may be written as

$$\bar{H}^{\Lambda}_{lm\lambda\mu}=0 \quad \text{if } mn-\mu\nu\neq(2Z+\lambda)\frac{N}{2}. \tag{45}$$

Now if λ is even, then $2Z+\lambda$ is an even integer, while if λ is odd $2Z+\lambda$ is an odd integer. Hence the inequality is equivalent to

$$\bar{H}^{\Lambda}_{lm\lambda\mu}=0 \quad \text{if } mn-\mu\nu\neq\frac{N}{2}Z_{\lambda}, \tag{46}$$

where Z_{λ} is an integer with the same parity as λ (i.e., if $\lambda=$even, then $Z_{\lambda}=0,\pm2,\pm4,...$; if $\lambda=$odd, then $Z_{\lambda}=\pm1,\pm3,\pm5,...$). The second order selection rule Eq. (43) may be derived by using similar arguments to those in Ref. 55.

The selection rules for $C(N/2)^{\nu}_{n}$ sequences are a subset of the selection rules for RN^{ν}_{n} sequences. This reflects the fact that the symmetry elements for $C(N/2)^{\nu}_{n}$ are a subgroup of the symmetry elements for RN^{ν}_{n} (see above).

In order to elucidate the use of these selection rules, consider the design of a γ-encoded homonuclear double-quantum recoupling sequence. A sequence of this type may be generated by imposing the following properties: (i) Terms with spin rank $\lambda=2$ and spin components $\mu=\pm2$ should be symmetry allowed in the first order average Hamiltonian. (ii) The term with $\mu=-2$ should be associated with only one spatial rotational component. (iii) All other homonuclear dipolar terms and all CSA terms should be suppressed. Solutions of the type RN^{ν}_{n} and CN^{ν}_{n} may be found by scanning through many combinations of symmetry numbers N, n, and υ and testing the conditions (i), (ii), and (iii) using Eqs. (40)

and (42). This search turns up a large number of possible solutions, including $C7_2^1$ (Ref. 11), $C14_4^5$ (Ref. 56), and $R14_2^6$ (Ref. 17).

I. Scaling factors

The magnitude of the symmetry-allowed terms depends on the pulse sequence. In general, a symmetry-allowed term in the first order effective Hamiltonian has the form

$$\bar{H}^{\Lambda}_{lm\lambda\mu} = \kappa_{lm\lambda\mu}[A^{\Lambda}_{lm}]^R \exp\{-im(\alpha^0_{RL} - \omega_r t^0_0)\} T^{\Lambda}_{\lambda\mu}. \quad (47)$$

Note that the phase of $\bar{H}^{\Lambda}_{lm\lambda\mu}$ depends on the starting time point t^0_0 of the pulse sequence. The scaling factor $\kappa_{lm\lambda\mu}$ of the symmetry-allowed term with quantum numbers (l,m,λ,μ) is given by

$$\kappa_{lm\lambda\mu} = d^l_{m0}(\beta_{RL})\,\tau_E^{-1} \int_{t^0_0}^{t^0_0+\tau_E} dt_0\; d^{\lambda}_{\mu 0}(-\beta_0) \times \exp\{i[\mu\gamma_0 + m\omega_r(t_0 - t^0_0)]\}. \quad (48)$$

The symbols t_0, β_0, and γ_0 refer to time points and rf Euler angles within the first pulse sequence element $\mathscr{E}_0$.

It is convenient to define the scaling factor with respect to the basic element $\mathscr{E}^0$ upon which the pulse sequence is constructed. The definition depends on whether a CN^{ν}_n or RN^{ν}_n sequence is applied:

(i) CN^{ν}_n *sequences*:

$$\kappa_{lm\lambda\mu} = d^l_{m0}(\beta_{RL}) K_{m\lambda\mu}. \quad (49)$$

(ii) RN^{ν}_n *sequences*:

$$\kappa_{lm\lambda\mu} = d^l_{m0}(\beta_{RL}) \exp\left\{-i\mu\frac{\pi\nu}{N}\right\} K_{m\lambda\mu}. \quad (50)$$

In both cases the factors $K_{m\lambda\mu}$ are defined with respect to the basic element $\mathscr{E}^0$, according to

$$K_{m\lambda\mu} = \tau_E^{-1} \int_0^{\tau_E} dt^0 d^{\lambda}_{\mu 0}(-\beta^0) \exp\{i(\mu\gamma^0 + m\omega_r t^0)\}. \quad (51)$$

The symbols t^0, β^0, and γ^0 refer to time points and rf Euler angles within the basic element $\mathscr{E}^0$.

The calculation of $K_{m\lambda\mu}$ for general basic elements $\mathscr{E}^0$ is discussed in Appendix B. In the specific case of amplitude modulated rf fields, the calculation is straightforward. If the basic element $\mathscr{E}^0$ consists of amplitude-modulated rf fields with phase 0 or π, the Euler angles are given by

$$\beta^0 = \int_0^{t^0} dt\,\omega_{\mathrm{nut}}(t), \quad \gamma^0 = \frac{\pi}{2}. \quad (52)$$

Here $\omega_{\mathrm{nut}}(t)$ is the rf field amplitude expressed as a nutation frequency (negative values corresponding to phase π).

In general, if two symmetries CN^{ν}_n and $CN^{\nu'}_n$ allow the same term (l,m,λ,μ), then the scaling factor $\kappa_{lm\lambda\mu}$ is the same for these two pulse sequences, providing the basic elements $\mathscr{E}^0$ are identical. If two sequences RN^{ν}_n and $RN^{\nu'}_n$ allow the same term, on the other hand, then the two scaling factors $\kappa_{lm\lambda\mu}$ have the same amplitude but differ by a phase factor, if the basic elements are identical.

J. Pulse sequence propagators

The effective propagator of the pulse sequence may be approximated using the first and second order approximation for the effective Hamiltonian. Strictly, the effective Hamiltonians propagates the spin system from the time point t^0_0 to the time point $t^0_0 + T$. However, if the internal spin interactions are not too large, the average Hamiltonian is often found to be a good approximation for intermediate time points as well. In this case, the propagators up to time point t^0_q are given by

(i) CN^{ν}_n *sequences*:

$$\bar{U}(t^0_q, t^0_0) \approx R_x(qZ_g\pi)\exp\{-i(\bar{H}^{(1)} + \bar{H}^{(2)})q\tau_E\}. \quad (53)$$

(ii) RN^{ν}_n *sequences*:

$$\bar{U}(t^0_q, t^0_0) \approx R_x(qZ_u\pi)R_z\left(-\frac{2\pi\nu}{N}q\right)\exp\{-i(\bar{H}^{(1)} + \bar{H}^{(2)})q\tau_E\}. \quad (54)$$

Note that the first and second order average Hamiltonians $\bar{H}^{(1)}$ and $\bar{H}^{(2)}$ depend on the starting time point t^0_0 of the pulse sequence.

The results discussed above allow the design of a variety of rotor-synchronized pulse sequences for many different purposes is solid state NMR.[17,55,56] In the following, these concepts are generalized to rf fields applied simultaneously to two rf channels.

III. DUAL ROTOR-SYNCHRONIZED PULSE SEQUENCES

In the following we discuss a number of different classes of rotor-synchronized rf pulse sequences which are applied simultaneously at the Larmor frequencies of one or two different spin species, denoted *S* and *K*. For example, *S* and *K* may comprise two rare spin species, immersed in a pool of abundant spins, denoted *I*. One common case is $S = {}^{13}C$, $K = {}^{15}N$, and $I = {}^{1}H$. In the following we assume that the abundant *I* spins are decoupled from the rare *S* and *K* spins by the application of a suitably modulated strong rf field at the *I*-spin Larmor frequency.

A. Heteronuclear spin interactions

In a system of coupled *S* and *K* spins the internal spin Hamiltonian at time point *t* may be written

$$H_{\mathrm{int}}(t) = \sum_{\Lambda,l,m,\lambda_S,\lambda_K} H^{\Lambda}_{lm\lambda_S 0\lambda_K 0}(t), \quad (55)$$

where the symbol Λ represents the type of interaction (chemical shift, homonuclear spin-spin coupling, heteronuclear spin–spin coupling) and also the indices of the spins involved in the interaction. As before, the sum over the parameter Λ runs over the different interactions (homo- and heteronuclear) as well as over the relevant spin indices. The term $H^{\Lambda_{SK}}_{lm\lambda_S\mu_S\lambda_K\mu_K}(t)$ includes both homo- and heteronuclear interactions for the *S* and *K* spins:

TABLE III. Heteronuclear spin interactions in a solid rotating at the magic angle with respect to the external magnetic field, and their properties with respect to spatial and spin rotations. The spatial components with $m=0$ disappear for exact magic-angle spinning, in the case $l=2$.

			S		K	
Interaction	Space rank l	Space component m	Spin rank λ_S	Spin component μ_S	Spin rank λ_K	Spin component μ_K
heteronuclear dipolar coupling	2	$-2, -1, 1, 2$	1	$-1, 0, 1$	1	$-1, 0, 1$
heteronuclear isotropic J coupling	0	0	1	$-1, 0, 1$	1	$-1, 0, 1$

$$H^{\Lambda}_{lm\lambda_S\mu_S00}(t)=H^{\Lambda_S}_{lm\lambda_S\mu_S}(t), \tag{56}$$

$$H^{\Lambda}_{lm00\lambda_K\mu_K}(t)=H^{\Lambda_K}_{lm\lambda_K\mu_K}(t), \tag{57}$$

$$H^{\Lambda_{SK}}_{lm\lambda_S\mu_S\lambda_K\mu_K}(t)=\sum_{\Lambda_{SK},l,m,\lambda_S,\mu_S,\lambda_K,\mu_K}\omega^{\Lambda_{SK}}_{lm}\exp\{im\omega_r t\}\times T^{\Lambda_S}_{\lambda_S\mu_S}T^{\Lambda_K}_{\lambda_K\mu_K}. \tag{58}$$

The sum over Λ_{SK} is taken over all heteronuclear interactions and all relevant heteronuclear spin pairs. The term $H^{\Lambda_{SK}}_{lm\lambda_S\mu_S\lambda_K\mu_K}(t)$ transforms as an irreducible spherical tensor of rank l for spatial rotations, rank λ_S for S-spin rotations, and rank λ_K for K-spin rotations. The components indices m, μ_S, and μ_K have values $m=-l,-l+1,...,l$ for space, $\mu_S=-\lambda_S,-\lambda_S+1,...,\lambda_S$ for S spins, and $\mu_K=-\lambda_K,-\lambda_K+1,...,\lambda_K$ for K spins. Table III contains a list of heteronuclear interactions and the corresponding values for the ranks l, λ_S, and λ_K, and components m, μ_S, and μ_K, under magic-angle rotation of the sample.

The modulation amplitudes $\omega^{\Lambda_{SK}}_{lm}$ of the heteronuclear interactions are written as before as

$$\omega^{\Lambda_{SK}}_{lm}=[A^{\Lambda_{SK}}_{lm}]^R d^l_{m0}(\beta_{RL})\exp\{-im\alpha^0_{RL}t\}, \tag{59}$$

where the amplitudes of the rank l tensor of interaction Λ_{SK} may be transformed from the principle axis frame to the rotor fixed frame through the usual chain of transformations:

$$[A^{\Lambda_{SK}}_{lm}]^R=\sum_{m'm''}[A^{\Lambda_{SK}}_{lm''}]^P D^l_{m''m'}(\Omega^{\Lambda_{SK}}_{PM})D^l_{m'm}(\Omega_{MR}). \tag{60}$$

The Euler angles $\Omega^{\Lambda_{SK}}_{PM}$ orient the principle axis frame of the heteronuclear interaction with respect to the molecular axis frame.

B. Classification of dual synchronized pulse sequences

There exist four different possibilities for applying the CN^{ν}_n and RN^{ν}_n sequences simultaneously at the Larmor frequency of the S and K spins (Fig. 2) In each case the number of basic elements N and the total number of rotor periods n is the same in each sequence. However, the phase increment parameter ν and the symmetry class C or R may be different for the two channels. The basic elements $\mathscr{E}^0_S$ and $\mathscr{E}^0_K$ may also be different on the two channels, even if both channels employ the same type of symmetry. The spin winding numbers ν for the S and K spins are denoted ν_S and ν_K, respectively. The following combinations are possible.

(a) S:$CN^{\nu_S}_n$,K:$CN^{\nu_K}_n$. This type of synchronized dual C sequence is denoted CN^{ν_S,ν_K}_n.
(b) S:$CN^{\nu_S}_n$,K:$RN^{\nu_K}_n$. This type of mixed C and R sequence is denoted CRN^{ν_S,ν_K}_n.
(c) S:$RN^{\nu_S}_n$,K:$CN^{\nu_K}_n$. This type of mixed R and C sequence is denoted RCN^{ν_S,ν_K}_n.
(d) S:$RN^{\nu_S}_n$,K:$RN^{\nu_K}_n$. This type of synchronized dual R sequence is denoted RN^{ν_S,ν_K}_n.

The symmetries of the Euler angles under the rf fields are analogous to those for the single channel rotor-synchronized sequences. For example, for a CRN^{ν_S,ν_K}_n sequence, the rf Euler angles obey the symmetries

$$\beta^S_q=\beta^S_0, \qquad \beta^K_q=\beta^K_0+q\pi, \tag{61}$$

$$\gamma^S_q=\gamma^S_0-\frac{2\pi\nu_S}{N}q, \quad \gamma^K_q=\gamma^K_0-\frac{2\pi\nu_K}{N}q, \tag{62}$$

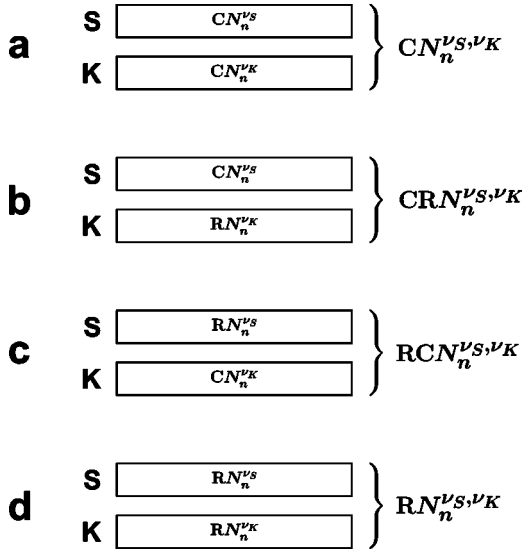

FIG. 2. Possibilities of dual RN^{ν}_n and CN^{ν}_n sequences in a heteronuclear spin system composed of species S and K. (a) A CN^{ν_S,ν_K}_n sequence. (b) A CRN^{ν_S,ν_K}_n sequence. (c) A RCN^{ν_S,ν_K}_n sequence. (d) A RN^{ν_S,ν_K}_n sequence.

where the rf propagators on the two channels are expressed as

$$U_{\mathrm{rf}}^{S}(t,t_0^0)=R_z^S[\alpha^S(t)]R_y^S[\beta^S(t)]R_z^S[\gamma^S(t)], \tag{63}$$

$$U_{\mathrm{rf}}^{K}(t,t_0^0)=R_z^K[\alpha^K(t)]R_y^K[\beta^K(t)]R_z^K[\gamma^K(t)], \tag{64}$$

and $R_\chi^S=\exp\{-i\phi S_\chi\}$ is the operator for a rotation of all S spins around the rotating-frame axis $\chi=(x,y,z)$ through the angle ϕ. $R_\chi^K=\exp\{-i\phi K_\chi\}$ is the corresponding K-spin rotation operator. As usual the notation β_q^S indicates $\beta^S(t_q)$, where t_q is a time point in the interval $[t_q^0,t_{q+1}^0]$, and similarly for $\gamma_q^S,\beta_q^K,\gamma_q^K$.

Analogous to the single-channel case, the Euler angles α_S^0, β_S^0, and γ_S^0 refer to the accumulated S-spin rf rotation up to a time point t^0 within the basic element $\mathscr{E}_S^0$, whereas the Euler angles α_K^0, β_K^0, and γ_K^0 refer to the accumulated K-spin rf rotation up to a time point t^0 within the basic element $\mathscr{E}_K^0$.

C. Interaction frame symmetry

As in the single-channel case, the terms of Eq. (55) maybe transformed into the interaction frame of the two rf fields at the Larmor frequencies of the S and K spins:

$$\tilde{H}(t)=\sum_{\Lambda,l,m,\lambda_S,\mu_S,\lambda_K,\mu_K}\tilde{H}^{\Lambda}_{lm\lambda_S\mu_S\lambda_K\mu_K}(t), \tag{65}$$

where μ_S and μ_K take all possible values, $\mu_S=-\lambda_S,\ -\lambda_S+1,...,\ \lambda_S$, and $\mu_K=-\lambda_K,-\lambda_K+1,...,\lambda_K$. The terms for $\mu_S=\lambda_S=0$ and $\mu_K=\lambda_K=0$ are the same as those defined in the single channel case:

$$\tilde{H}^{\Lambda}_{lm\lambda_S\mu_S00}(t)=\tilde{H}^{\Lambda_S}_{lm\lambda_S\mu_S}(t), \tag{66}$$

$$\tilde{H}^{\Lambda}_{lm00\lambda_K\mu_K}(t)=\tilde{H}^{\Lambda_K}_{lm\lambda_K\mu_K}(t). \tag{67}$$

The symmetries of the interaction frame terms may be deduced by a straightforward extension of the results given in the previous section. The relevant symmetries are

(i) $\mathrm{CN}_n^{\nu_S,\nu_K}$ *sequences*:

$$\tilde{H}^{\Lambda}_{lm\lambda_S\mu_S\lambda_K\mu_K}(t_q)=\tilde{H}^{\Lambda}_{lm\lambda_S\mu_S\lambda_K\mu_K}(t_0)\exp\left\{i\frac{2\pi q}{N}(mn-\mu_S\nu_S-\mu_K\nu_K)\right\}. \tag{68}$$

(ii) $\mathrm{CRN}_n^{\nu_S,\nu_K}$ *sequences*:

$$\tilde{H}^{\Lambda}_{lm\lambda_S\mu_S\lambda_K\mu_K}(t_q)=\tilde{H}^{\Lambda}_{lm\lambda_S\mu_S\lambda_K\mu_K}(t_0)\exp\left\{i\frac{2\pi q}{N}\left(mn-\mu_S\nu_S-\mu_K\nu_K-\frac{\lambda_K N}{2}\right)\right\}. \tag{69}$$

(iii) $\mathrm{RCN}_n^{\nu_S,\nu_K}$ *sequences*:

$$\tilde{H}^{\Lambda}_{lm\lambda_S\mu_S\lambda_K\mu_K}(t_q)=\tilde{H}^{\Lambda}_{lm\lambda_S\mu_S\lambda_K\mu_K}(t_0)\exp\left\{i\frac{2\pi q}{N}\left(mn-\mu_S\nu_S-\mu_K\nu_K-\frac{\lambda_S N}{2}\right)\right\}. \tag{70}$$

(iv) $\mathrm{RN}_n^{\nu_S,\nu_K}$ *sequences*:

$$\tilde{H}^{\Lambda}_{lm\lambda_S\mu_S\lambda_K\mu_K}(t_q)=\tilde{H}^{\Lambda}_{lm\lambda_S\mu_S\lambda_K\mu_K}(t_0)\exp\left\{i\frac{2\pi q}{N}\left(mn-\mu_S\nu_S-\mu_K\nu_K-\frac{(\lambda_S+\lambda_K)N}{2}\right)\right\}. \tag{71}$$

D. Average Hamiltonian

The average Hamiltonian terms are given by

$$\bar{H}^{(1)}=\sum_{\Lambda,l,m,\lambda_S,\mu_S,\lambda_K,\mu_K}\tilde{H}^{\Lambda}_{lm\lambda_S\mu_S\lambda_K\mu_K}, \tag{72}$$

where

$$\bar{H}^{\Lambda}_{lm\lambda_S\mu_S\lambda_K\mu_K}=T^{-1}\int_{t_0^0}^{t_0^0+T}dt\tilde{H}^{\Lambda}_{lm\lambda_S\mu_S\lambda_K\mu_K}(t) \tag{73}$$

and

$$\bar{H}^{(2)}=\sum_{\Lambda_2,\mathbf{2},\Lambda_1,\mathbf{1}}\bar{H}^{\Lambda_2\times\Lambda_1}_{\mathbf{2};\mathbf{1}}, \tag{74}$$

where the vectors **1** and **2** represent the quantum numbers $(l_1,m_1,\lambda_{S1},\mu_{S1},\lambda_{K1},\mu_{K1})$ and $(l_2,m_2,\lambda_{S2},\mu_{S2},\lambda_{K2},\mu_{K2})$, respectively. The terms $\bar{H}^{\Lambda_2\times\Lambda_1}_{\mathbf{2};\mathbf{1}}$ are given by

$$\bar{H}^{\Lambda_2\times\Lambda_1}_{\mathbf{2};\mathbf{1}}=(2iT)^{-1}\int_{t_0^0}^{t_0^0+T}dt'\int_{t_0^0}^{t'}dt\times[\tilde{H}^{\Lambda_2}_{l_2m_2\lambda_{S2}\mu_{S2}\lambda_{K2}\mu_{K2}}(t'),\tilde{H}^{\Lambda_1}_{l_1m_1\lambda_{S1}\mu_{S1}\lambda_{K1}\mu_{K1}}(t)]. \tag{75}$$

The relevant symmetries of $\bar{H}^{(1)}$ and $\bar{H}^{(2)}$ for the four different sequence classes are

(i) $\mathrm{CN}_n^{\nu_S,\nu_K}$ *sequences*:

$$\bar{H}^{\Lambda}_{lm\lambda_S\mu_S\lambda_K\mu_K}=0 \quad \text{if } mn-\mu_S\nu_S-\mu_K\nu_K\neq NZ, \tag{76}$$

$$\bar{H}^{\Lambda_2\times\Lambda_1}_{\mathbf{2};\mathbf{1}}=0 \ \text{ if } \begin{cases} m_1n-\mu_{S1}\nu_S-\mu_{K1}\nu_K\neq NZ \\ \text{AND} \\ m_2n-\mu_{S2}\nu_S-\mu_{K2}\nu_K\neq NZ \\ \text{AND} \\ (m_2+m_1)n-(\mu_{S2}+\mu_{S1})\nu_S \\ \quad -(\mu_{K2}+\mu_{K1})\nu_K\neq NZ. \end{cases} \tag{77}$$

(ii) $\mathrm{CRN}_n^{\nu_S,\nu_K}$ *sequences*:

$$\bar{H}^{\Lambda}_{lm\lambda_S\mu_S\lambda_K\mu_K}=0 \quad \text{if } mn-\mu_S\nu_S-\mu_K\nu_K\neq\frac{N}{2}Z_{\lambda_K}, \tag{78}$$

$$\bar{H}^{\Lambda_2\times\Lambda_1}_{\mathbf{2;1}}=0 \quad \text{if} \begin{cases} m_1 n-\mu_{S1}\nu_S-\mu_{K1}\nu_K\neq\dfrac{N}{2}Z_{\lambda_{K1}} \\ \text{AND} \\ m_2 n-\mu_{S2}\nu_S-\mu_{K2}\nu_K\neq\dfrac{N}{2}Z_{\lambda_{K2}} \\ \text{AND} \\ (m_2+m_1)n-(\mu_{S2}+\mu_{S1})\nu_S \\ \quad -(\mu_{K2}+\mu_{K1})\nu_K\neq\dfrac{N}{2}Z_{\lambda_{K2}+\lambda_{K1}}. \end{cases} \tag{79}$$

(iii) $\mathrm{RCN}_n^{\nu_S,\nu_K}$ *sequences*:

$$\bar{H}^{\Lambda}_{lm\lambda_S\mu_S\lambda_K\mu_K}=0 \quad \text{if } mn-\mu_S\nu_S-\mu_K\nu_K\neq\frac{N}{2}Z_{\lambda_S}, \tag{80}$$

$$\bar{H}^{\Lambda_2\times\Lambda_1}_{\mathbf{2;1}}=0 \quad \text{if} \begin{cases} m_1 n-\mu_{S1}\nu_S-\mu_{K1}\nu_K\neq\dfrac{N}{2}Z_{\lambda_{S1}} \\ \text{AND} \\ m_2 n-\mu_{S2}\nu_S-\mu_{K2}\nu_K\neq\dfrac{N}{2}Z_{\lambda_{S2}} \\ \text{AND} \\ (m_2+m_1)n-(\mu_{S2}+\mu_{S1})\nu_S \\ \quad -(\mu_{K2}+\mu_{K1})\nu_K\neq\dfrac{N}{2}Z_{\lambda_{S2}+\lambda_{S1}}. \end{cases} \tag{81}$$

(iv) $\mathrm{RN}_n^{\nu_S,\nu_K}$ *sequences*:

$$\bar{H}^{\Lambda}_{lm\lambda_S\mu_S\lambda_K\mu_K}=0 \quad \text{if } mn-\mu_S\nu_S-\mu_K\nu_K\neq\frac{N}{2}Z_{\lambda_S+\lambda_K}, \tag{82}$$

$$\bar{H}^{\Lambda_2\times\Lambda_1}_{\mathbf{2;1}}=0 \quad \text{if} \begin{cases} m_1 n-\mu_{S1}\nu_S-\mu_{K1}\nu_K\neq\dfrac{N}{2}Z_{\lambda_{S1}+\lambda_{K1}} \\ \text{AND} \\ m_2 n-\mu_{S2}\nu_S-\mu_{K2}\nu_K\neq\dfrac{N}{2}Z_{\lambda_{S2}+\lambda_{K2}} \\ \text{AND} \\ (m_2+m_1)n-(\mu_{S2}+\mu_{S1})\nu_S \\ \quad -(\mu_{K2}+\mu_{K1})\nu_K\neq\dfrac{N}{2}Z_{\lambda_{S2}+\lambda_{S1}+\lambda_{K2}+\lambda_{K1}}. \end{cases} \tag{83}$$

The selection rules for $\bar{H}^{(1)}$ permit a classification of the pulse sequences on the basis of their recoupling and decoupling properties. The selection rules for $\bar{H}^{(2)}$ allow the prediction of the number and type of symmetry-allowed higher-order terms. These terms often determine the practical performance of the pulse sequences.[55]

E. Scaling factors

The magnitude of the symmetry allowed terms depends on the pulse sequence. In general, a symmetry allowed term in the first order effective Hamiltonian has the form

$$\bar{H}^{\Lambda}_{lm\lambda_S\mu_S00}=\bar{H}^{\Lambda_S}_{lm\lambda_S\mu_S}, \tag{84}$$

$$\bar{H}^{\Lambda}_{lm00\lambda_K\mu_K}=\bar{H}^{\Lambda_K}_{lm\lambda_K\mu_K}, \tag{85}$$

$$\bar{H}^{\Lambda}_{lm\lambda_S\mu_S\lambda_K\mu_K}=\kappa^{SK}_{lm\lambda_S\mu_S\lambda_K\mu_K}[A^{\Lambda_{SK}}_{lm}]^R\exp\{-im(\alpha^0_{RL}-\omega_r t^0_0)\} \times T^{\Lambda_S}_{\lambda_S\mu_S}T^{\Lambda_K}_{\lambda_K\mu_K}, \tag{86}$$

where $\kappa^{SK}_{lm\lambda_S\mu_S\lambda_K\mu_K}$ is the scaling factor of the symmetry-allowed term with the quantum numbers $(l,m,\lambda_S,\mu_S,\lambda_K,\mu_K)$ given by

$$\kappa^{SK}_{lm\lambda_S\mu_S\lambda_K\mu_K}=d^l_{m0}(\beta_{RL})\tau_E^{-1}\int_{t_0^0}^{t_1^0}dt_0\; d^{\lambda_S}_{\mu_S0}(-\beta_0^S)d^{\lambda_K}_{\mu_K0}(-\beta_0^K) \times\exp\{i[\mu_S\gamma_0^S+\mu_K\gamma_0^K+m\omega_r(t_0-t_0^0)]\}. \tag{87}$$

The symbols t_0, β_0^S, β_0^K, γ_0^S, and γ_0^K refer to time points and rf Euler angles within the first pulse sequence element.

It is convenient to define the scaling factor with respect to the basic elements $\mathscr{E}_S^0$ and $\mathscr{E}_K^0$.

(i) $\mathrm{CN}_n^{\nu_S,\nu_K}$ *sequences*:

$$\kappa^{SK}_{lm\lambda_S\mu_S\lambda_K\mu_K}=d^l_{m0}(\beta_{RL})K^{SK}_{m\lambda_S\mu_S\lambda_K\mu_K}. \tag{88}$$

(ii) $\mathrm{CRN}_n^{\nu_S,\nu_K}$ *sequences*:

$$\kappa^{SK}_{lm\lambda_S\mu_S\lambda_K\mu_K}=d^l_{m0}(\beta_{RL})\exp\left\{-i\mu_K\frac{\pi\nu_K}{N}\right\}K^{SK}_{m\lambda_S\mu_S\lambda_K\mu_K}. \tag{89}$$

(iii) $\mathrm{RCN}_n^{\nu_S,\nu_K}$ *sequences*:

$$\kappa^{SK}_{lm\lambda_S\mu_S\lambda_K\mu_K}=d^l_{m0}(\beta_{RL})\exp\left\{-i\mu_S\frac{\tau\nu_S}{N}\right\}K^{SK}_{m\lambda_S\mu_S\lambda_K\mu_K}. \tag{90}$$

(iv) $\mathrm{RN}_n^{\nu_S,\nu_K}$ *sequences*:

$$K^{SK}_{lm\lambda_S\mu_S\lambda_K\mu_K}=d^l_{m0}(\beta_{RL})\exp\left\{-i\left(\mu_S\frac{\pi\nu_S}{N}+\mu_K\frac{\pi\nu_K}{N}\right)\right\} \times K^{SK}_{m\lambda_S\mu_S\lambda_K\mu_K}, \tag{91}$$

where $K^{SK}_{m\lambda_S\mu_S\lambda_K\mu_K}$ is defined with respect to the basic elements $\mathscr{E}_S^0$ and $\mathscr{E}_K^0$ and is given by

$$K^{SK}_{m\lambda_S\mu_S\lambda_K\mu_K}=\tau_E^{-1}\int_0^{\tau_E}dt^0 d^{\lambda_S}_{\mu_S0}(-\beta_S^0)d^{\lambda_K}_{\mu_K0}(-\beta_K^0) \times\exp\{i(\mu_S\gamma_S^0+\mu_K\gamma_K^0+m\omega_r t^0)\}. \tag{92}$$

The symbols t^0, β_S^0, β_K^0, γ_S^0, and γ_K^0 refer to time points and rf Euler angles within the basic elements $\mathscr{E}_S^0$ and $\mathscr{E}_K^0$.

The calculation of the term $K^{SK}_{m\lambda_S\mu_S\lambda_K\mu_K}$ for general basic elements $\mathscr{E}_S^0$ and $\mathscr{E}_K^0$ is discussed in Appendix B. In the specific case of amplitude modulated rf fields, the calculation is straightforward. If the basic elements $\mathscr{E}_S^0$, $\mathscr{E}_K^0$ consist of amplitude-modulated rf fields with phase 0 and π, the Euler angles are given by

$$\beta_S^0=\int_0^{t^0} dt\,\omega_{\rm nut}^S(t), \quad \beta_K^0=\int_0^{t^0} dt\,\omega_{\rm nut}^K(t), \tag{93}$$

$$\gamma_S^0=\frac{\pi}{2}, \qquad \gamma_K^0=\frac{\pi}{2}. \tag{94}$$

Here $\omega_{\rm nut}^S(t)$ and $\omega_{\rm nut}^K(t)$ are the rf field amplitudes expressed as nutation frequencies (negative values corresponding to phase π).

F. Pulse sequence propagators

The effective propagator of the pulse sequence may be expressed in terms of the first and second order average Hamiltonian terms:

(i) $CN_n^{\nu_S,\nu_K}$ *sequences*:

$$\bar{U}(t_q^0,t_0^0)\approx R_x^S(qZ_g^S\pi)R_x^K(qZ_g^K\pi)\exp\{-i(\bar{H}^{(1)}+\bar{H}^{(2)})q\tau_E\}. \tag{95}$$

(ii) $CRN_n^{\nu_S,\nu_K}$ *sequences*:

$$\bar{U}(t_q^0,t_0^0)\approx R_x^S(qZ_g^S\pi)R_x^K(qZ_u^K\pi)R_z^K\left(-\frac{2\pi\nu_K}{N}q\right) \times\exp\{-i(\bar{H}^{(1)}+\bar{H}^{(2)})q\tau_E\}. \tag{96}$$

(iii) $RCN_n^{\nu_S,\nu_K}$ *sequences*:

$$\bar{U}(t_q^0,t_0^0)\approx R_x^S(qZ_u^S\pi)R_z^S\left(-\frac{2\pi\nu_S}{N}q\right)R_x^K(qZ_g^K\pi) \times\exp\{-i(\bar{H}^{(1)}+\bar{H}^{(2)})q\tau_E\}. \tag{97}$$

(iv) $RN_n^{\nu_S,\nu_K}$ *sequences*:

$$\bar{U}(t_q^0,t_0^0)\approx R_x^S(qZ_u^S\pi)R_z^S\left(-\frac{2\pi\nu_S}{N}q\right)R_x^K(qZ_u^K\pi) \times R_z^K\left(-\frac{2\pi\nu_K}{N}q\right)\exp\{-i(\bar{H}^{(1)}+\bar{H}^{(2)})q\tau_E\}, \tag{98}$$

where Z_g^S, Z_g^K are even integers and Z_u^S, Z_u^K are odd integers.

In the following section these results will be applied to the problem of heteronuclear recoupling of two spin species.

IV. SELECTIVE HETERONUCLEAR RECOUPLING

A. Types of heteronuclear recoupling

There are several different types of average Hamiltonians which achieve heteronuclear recoupling. The choice of pulse sequence depends not only on the form of the recoupled interactions but also on the removal of unwanted terms in the average Hamiltonian and on the desirability of γ encoding. In this paper we concentrate on the design of γ-encoded rf pulse sequences which recouple the heteronuclear dipolar interactions, but which also decouple all the homonuclear dipolar interactions, all isotropic chemical shifts, and all chemical shift anisotropies. In the following we discuss the generation of several possible average Hamiltonians suitable for heteronuclear recoupling. We use the term *generalized Hartmann–Hahn* sequence to refer to rotor-synchronized heteronuclear recoupling sequences which involve rf irradiation at the Larmor frequencies of both involved spin species.

1. REDOR-type recoupling

One possible form for the recoupled heteronuclear average Hamiltonian is as follows:

$$\bar{H}_{SK}^{(1)}=\sum_{s<k}\omega_{sk}S_{sz}K_{kz}, \tag{99}$$

where the sum is taken over all heteronuclear spin pairs. In this case $\mu_S=\mu_K=0$. Such an average Hamiltonian is, for example, generated by a REDOR sequence applied to one of the spin species.[3,4] One advantage of this type of average Hamiltonian is that the terms $S_{sz}K_{kz}$ commute for different spin pairs. This means the evolution of the heteronuclear spin system can be described as the superposition of the evolution of isolated spin pairs. One disadvantage of such a Hamiltonian is that it cannot be γ encoded because the term for $(\mu_S,\mu_K)=(0,0)$ is always associated with both the $m=\pm1$ components and/or both the $m=\pm2$ components. The lack of γ encoding reduces the amplitude of dipolar oscillations in powdered samples and makes quantitative distance measurements more difficult.

Another issue is the possible influence of recoupled homonuclear dipolar interactions and CSA interactions.

If CN_n^ν or RN_n^ν sequences are applied on a single rf channel, it is not possible to decouple the CSA interaction of the irradiated spins at the same time as recoupling the heteronuclear dipolar interactions, since these terms have the same symmetry properties under rotations of a single spin species. As a result, any single-channel CN_n^ν or RN_n^ν sequence applied to the K spins necessarily recouples the $\mu_K=0$ components of the K-spin CSA if it is designed to recouple the $\mu_S=\mu_K=0$ components of the SK dipolar interactions. However, these recoupled SK and K-spin CSA interactions commute, so this particular recoupling effect is relatively harmless.

It is possible to generate a recoupled heteronuclear dipolar Hamiltonian of the form of Eq. (99), at the same time as decoupling the homonuclear dipolar interactions of the irradiated spins. Some suitable single-channel symmetries are $R12_3^1$, $R12_3^2$, $R12_3^4$, $R12_3^5$, $R16_4^1$, $R16_4^5$, $R16_4^7$, $R20_5^1$, $R20_5^9$, etc. All of these solutions suppress isotropic chemical shift terms in the first order average Hamiltonian, but also recouple the CSA interactions of the irradiated spins, as mentioned above. In addition, the recoupled heteronuclear dipolar interaction is not γ encoded. These solutions may be regarded as variants of REDOR with four π pulses per rotor period instead of two. A similar effect is achieved by the recently described C-REDOR sequences,[48] which are based on CN_n^ν symmetries.

The standard REDOR sequence[3,4] can also be viewed in the framework of the RN_n^ν sequences. For example, the phases of the 180° pulses in the REDOR sequences have phases 0°, 90°, 0°, 90°, if the XY-4 phase cycle[67] is used. This case is therefore equivalent to four 180° pulses in two rotor periods with the phases −45°, +45°, −45°, +45°.

REDOR together with the XY-4 phase cycle can therefore be viewed as an $R4_2^{-1}$ sequence, because $\pi\nu/N=-45°$ in this case. If the XY-8 phase cycle[67] is used for the 180° pulses, REDOR is equivalent to the supercycled sequence $R4_2^{-1}R4_2^1$. In the case of the XY-16 phase cycle[67] REDOR is equivalent to the supercycle $[R4_2^{-1}R4_2^1]_0[R4_2^{-1}R4_2^1]_{180}$. The symmetry analysis of $R4_2^1$ shows that in general a REDOR sequence applied to the *K* spins also recouples the *K*-spin homonuclear dipolar interactions. Since REDOR conforms to $R4_4^1$ symmetry, the choice of the π pulse element only effects the scaling factor, in first order average Hamiltonian theory. This explains the successful use of REDOR at high spinning frequencies.[46]

The two-channel selection rules in Eqs. (76), (78), (80), and (82) do not give rise to any solutions in which the $\mu_S=\mu_K=0$ heteronuclear dipolar terms are recoupled, at the same time as all homonuclear dipolar coupling terms are removed. On the other hand, dual sequences do make it possible to remove all chemical shift anisotropy terms in the first order average Hamiltonian at the same time as achieving a heteronuclear dipolar Hamiltonian of the form given in Eq. (99). So far we did not explore this class of solutions further.

2. Single-quantum heteronuclear recoupling

Another possible form for the recoupled heteronuclear average Hamiltonian is

$$\overline{H}_{SK}^{(1)}=\sum_{s<K}(\omega_{sk}S_{sz}K_k^-+\omega_{sk}^*S_{sz}K_k^+). \tag{100}$$

This type of Hamiltonian may be generated by applying RN_n^ν sequences to the *K*-spin species, as discussed in Refs. 17 and 68. However, these symmetries also recouple the *K*-spin CSA, and the recoupled *K*-spin CSA and *SK* dipolar interaction do not in general commute. Another possibility is to use dual $RN_n^{\nu_S,\nu_K}$ sequences, where the chemical shift anisotropy is removed for both spin species in the first order average Hamiltonian. Some solutions of this kind are $R10_2^{5,2}$, $R8_3^{4,3}$, $R10_3^{5,3}$, $R14_3^{2,3}$, and $R16_3^{1,3}$, which all recouple the terms $(m,\mu_S,\mu_K)=(1,0,1)$ and $(-1,\ 0,\ -1)$. However, these solutions all recouple the *K*-spin homonuclear dipolar interactions as well as the *SK* heteronuclear dipolar interactions. We did not investigate these sequences further.

3. Double-quantum heteronuclear recoupling

The following heteronuclear recoupled Hamiltonian also has a favorable form:

$$\overline{H}_{SK}^{(1)}=\sum_{s<k}(\omega_{sk}S_s^-K_k^-+\omega_{sk}^*S_s^+K_k^+). \tag{101}$$

This type of selective recoupling cannot be achieved by applying an rf pulse sequence to only one of the two spin species.

A dual-channel rotor-synchronized pulse sequence, generating a γ-encoded average Hamiltonian of the type Eq. (101), is generated by imposing the following properties: (i) First order average Hamiltonian terms with spin ranks $(\lambda_S,\lambda_K)=(1,1)$ and spin components $(\mu_S,\mu_K)=(-1,-1)$ and (1, 1) should be symmetry allowed. (ii) The term with $(\mu_S,\mu_K)=(-1,-1)$ should be associated with only one spatial rotational component, denoted here m'. The term with $(\mu_S,\mu_K)=(1,1)$ is therefore associated with the space component $-m'$. (iii) All other heteronuclear dipolar interaction terms, all homonuclear dipolar interaction terms, and chemical shift anisotropy terms should be suppressed for both spin species *S* and *K*. Tables IV and V show some two-channel solutions which fulfill these conditions. All the symmetries in Tables IV and V represent generalized HH sequences which recouple the heteronuclear dipolar terms with $(m,\mu_S,\mu_K)=(1,-1,-1)$ and $(-1,\ 1,\ 1)$. There also exist solutions for $m=\pm2$, which are not shown here, because in general these sequences have a smaller scaling factor $\kappa_{lm\lambda_S\mu_S\lambda_K\mu_K}^{SK}$ for the recoupled heteronuclear dipolar interactions.

Table IV contains solutions of the type $CRN_n^{\nu_S,\nu_K}$. All these symmetries decouple the heteronuclear isotropic *J* coupling between the two spin species as well as imposing heteronuclear dipolar recoupling. The *K*-spin isotropic chemical shifts are also removed. Table V contains solutions of the type $RN_n^{\nu_S,\nu_K}$. All of these symmetries retain the $(m,\mu_S,\mu_K)=(0,0,0)$ component of the isotropic heteronuclear *J* coupling, as well as decoupling the isotropic chemical shifts of both spin species.

Figures 3 and 4 explain the operation of $R18_3^{7,8}$ in detail using space–spin selection diagrams (SSS diagrams) introduced in Ref. 56. For this case the selection rules Eqs. (42) and (82) apply.

Figure 3(a) indicates that the symmetry $R18_3^{7,8}$ blocks all homonuclear *K*-spin interactions in the first order average Hamiltonian. The levels in Fig. 3(a) indicate the total value of $mn-\mu_K\nu_K$. The superposition of mn and $-\mu_K\nu_K$ is broken into two stages, so as to separate the effects of spatial rotations and spin rotations of the *K* nuclei. The ''barriers'' on the right-hand side of each diagram have holes separated by *N* units. The positions of the holes are determined by the parity of λ_K, which corresponds to the inequality in the symmetry theorem Eq. (42). For the homonuclear dipolar couplings λ_K is even and therefore the position of each hole corresponds to an even multiple of $N/2$, i.e., 0, ±18, ±36,.... For the chemical shift anisotropy λ_K is odd so that the position of each hole corresponds to an odd multiple of $N/2$, i.e., ±9, ±27,.... Pathways which pass through a hole indicate space–spin components which are symmetry allowed in the first order average Hamiltonian. Figure 3(a) shows that $R18_3^8$ symmetry for the *K* spins suppresses all *K*-spin homonuclear dipolar coupling components ($m=\{\pm1,\pm2\}$ and $\mu_K=\{0,\pm1,\pm2\}$) and all *K*-spin CSA components ($m=\{\pm1,\pm2\}$ and $\mu_K=\{0,\pm1\}$) in the first order average Hamiltonian. This symmetry also suppresses all *K*-spin isotropic chemical shift terms ($m=0$ and $\mu_K=\{0,\pm1\}$).

TABLE IV. Inequivalent $\mathrm{CRN}_n^{\nu_S,\nu_K}$ sequences leading to γ-encoded heteronuclear double-quantum recoupling, with suppression of all chemical shift anisotropies and homonuclear dipolar coupling terms. The symmetry-allowed terms are in all cases given by $(m,\mu_S,\mu_K)=\{(1,-1,-1),(-1,1,1)\}$. Sequences with $N\leqslant 24$, $n\leqslant 9$, $N/n\leqslant 7$ are shown. If $(\nu_S,\nu_K)=(\nu_S',\nu_K')$ is a suitable solution, then (ν_K',ν_S') is also a suitable solution with the same symmetry-allowed terms. Sequences with symmetry-allowed terms given by $(m,\mu_S,\mu_K)=\{(1,1,1),(-1,-1,-1)\}$ may be constructed by reversing the sign of both ν_S' and ν_K'. All sequences decouple the heteronuclear isotropic J coupling and remove all K- spin isotropic chemical shift terms.

N	n	ν_S	ν_K	N	n	ν_S	ν_K
14	3	2	2	22	6	−2	7
14	3	−5	−5	22	6	−4	9
16	3	1	4	16	7	−3	4
16	3	−4	−7	16	7	−4	5
18	3	−1	7	18	7	−1	3
18	3	1	5	18	7	1	1
18	3	−2	8	18	7	−6	8
18	3	2	4	18	7	−8	−8
18	3	−4	−8	20	7	1	2
18	3	−5	−7	20	7	−2	5
20	3	−1	8	20	7	−5	8
20	3	−2	9	20	7	−8	−9
20	3	2	5	22	7	−1	5
20	3	−5	−8	22	7	−2	6
20	4	−1	7	22	7	2	2
20	4	1	5	22	7	−5	9
20	4	−3	9	22	7	−6	10
20	4	3	3	22	7	−9	−9
20	4	−5	−9	24	7	−1	6
20	4	−7	−7	24	7	1	4
22	4	1	6	24	7	−3	8
22	4	−5	−10	24	7	−4	9
24	4	−1	9	24	7	−6	11
24	4	1	7	24	7	−8	−11
24	4	−3	11	20	8	−1	3
24	4	3	5	20	8	1	1
24	4	−5	−11	20	8	−3	5
24	4	−7	−9	20	8	−5	7
14	5	1	1	20	8	−7	9
14	5	−6	−6	20	8	−9	−9
16	5	−1	4	22	8	1	2
16	5	−4	7	22	8	−9	−10
18	5	−2	6	14	9	−1	−1
18	5	2	2	14	9	6	6
18	5	−3	7	16	9	3	−4
18	5	−7	−7	16	9	4	−5
22	5	−2	8	20	9	−3	4
22	5	2	4	20	9	−4	5
22	5	−3	9	20	9	−5	6
22	5	3	3	20	9	−6	7
22	5	−7	−9	22	9	−1	3
22	5	−8	−8	22	9	1	1
24	5	−1	8	22	9	−3	5
24	5	1	6	22	9	−6	8
24	5	3	4	22	9	−8	10
24	5	−4	11	22	9	−10	−10
24	5	−6	−11	24	9	−1	4
24	5	−8	−9	24	9	1	2
16	6	1	1	24	9	−2	5
16	6	−7	−7	24	9	−4	7
20	6	−1	5	24	9	−5	8
20	6	−5	9	24	9	−7	10
				24	9	−8	11
				24	9	−10	−11

TABLE V. Inequivalent $R N_n^{\nu_S,\nu_K}$ sequences leading to γ-encoded heteronuclear double-quantum recoupling, with suppression of all isotropic chemical shift terms, chemical shift anisotropies, and homonuclear dipolar coupling terms. The symmetry-allowed terms are in all cases given by $(m,\mu_S,\mu_K)=\{(1,-1,-1),(-1,1,1)\}$. Sequences with $N\leqslant 24$, $n\leqslant 9$, $N/n\leqslant 7$ are shown. If $(\nu_S,\nu_K)=(\nu_S',\nu_K')$ is a suitable solution, then (ν_K',ν_S') is also a suitable solution with the same symmetry-allowed terms. Sequences with symmetry-allowed terms given by $(m,\mu_S,\mu_K)=\{(1,1,1),(-1,-1.-1)\}$ may be constructed by reversing the sign of both ν_S' and ν_K'. All sequences retain the $(m,\mu_S,\mu_K)=(0,0,0)$ component of the heteronuclear isotropic J coupling.

N	n	ν_S	ν_K	N	n	ν_S	ν_K
14	3	2	−5	22	6	−2	−4
				22	6	7	9
16	3	1	−4				
16	3	4	−7	16	7	−3	−4
				16	7	4	5
18	3	−1	−2				
18	3	1	−4	18	7	−1	−6
18	3	2	−5	18	7	1	−8
18	3	4	−7	18	7	3	8
18	3	5	−8				
18	3	7	8	20	7	1	−8
				20	7	−2	−5
20	3	−1	−2	20	7	2	−9
20	3	2	−5	20	7	5	8
20	3	5	−8				
20	3	8	9	22	7	−1	−6
				22	7	−2	−5
20	4	−1	−3	22	7	2	−9
20	4	1	−5	22	7	5	10
20	4	3	−7	22	7	6	9
20	4	5	−9				
20	4	7	9	24	7	−1	−6
				24	7	1	−8
22	4	1	−5	24	7	−3	−4
22	4	6	−10	24	7	4	−11
				24	7	6	11
24	4	−1	3	24	7	8	9
24	4	1	−5				
24	4	3	−7	20	8	−1	−7
24	4	5	−9	20	8	1	−9
24	4	7	−11	20	8	−3	−5
24	4	9	11	20	8	3	9
				20	8	5	7
14	5	1	−6				
				22	8	1	−9
16	5	−1	−4	22	8	2	−10
16	5	4	7				
				14	9	1	−6
18	5	−2	−3				
18	5	2	−7	16	9	3	4
18	5	6	7	16	9	−4	−5
22	5	−2	−3	20	9	−3	−6
22	5	2	−7	20	9	−4	−5
22	5	3	−8	20	9	4	7
22	5	4	−9	20	9	5	6
22	5	8	9				
				22	9	−1	−8
24	5	−1	−4	22	9	1	−10
24	5	1	−6	22	9	−3	−6
24	5	3	−8	22	9	3	10
24	5	4	−9	22	9	5	8
24	5	6	−11				
24	5	8	11	24	9	−1	−8
				24	9	1	−10
16	6	1	−7	24	9	−2	−7
				24	9	2	−11
20	6	−1	−5	24	9	−4	−5
20	6	5	9	24	9	4	11
				24	9	5	10
				24	9	7	8

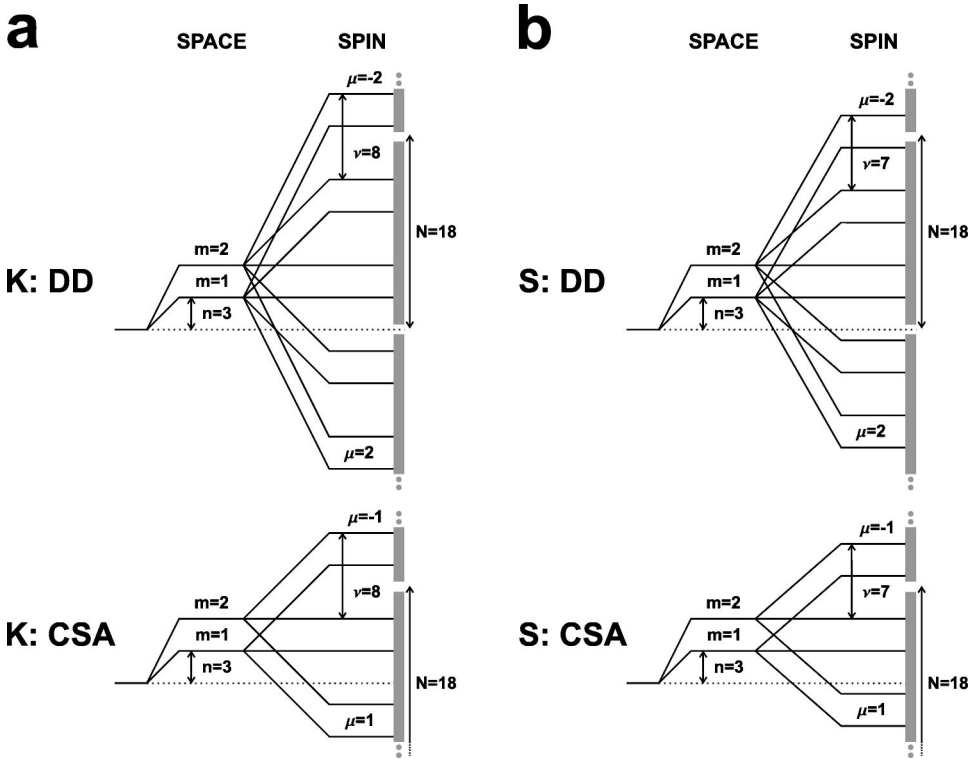

FIG. 3. Space–spin selection diagram for the dual $R18_3^{7,8}$ sequence. (a) Suppression of all CSA and homonuclear dipole–dipole coupling components for the K spins. (b) Suppression of all CSA and homonuclear dipole–dipole coupling components for the S spins. The mirror image pathways stemming from $m=-1$, $m=-2$ have been suppressed for simplicity.

Figure 3(b) shows the corresponding levels for the total value of $mn-\mu_S\nu_S$. This figure shows that the $R18_3^7$ symmetry for the S spins suppresses all S-spin homonuclear dipolar coupling components ($m=\{\pm1,\pm2\}$ and $\mu_S=\{0,\pm1,\pm2\}$) and all S-spin CSA components ($m=\{\pm1,\pm2\}$ and $\mu_S=\{0,\pm1\}$) in the first order average Hamiltonian. The S-spin isotropic chemical shift terms ($m=0$ and $\mu_S=\{0,\pm1\}$) are also suppressed.

Figure 4 shows the selection of heteronuclear couplings terms by the $R18_3^{7,8}$ sequence. The levels in Fig. 4 indicate the total value of $mn-\mu_S\nu_S-\mu_K\nu_K$ broken into three stages. The barrier at the right-hand side has holes separated by N units, corresponding to Eq. (82). The position of the holes is determined by the parity of the sum $\lambda_S+\lambda_K$. For heteronuclear dipolar couplings $\lambda_S+\lambda_K$ is even and therefore the holes are placed at even multiples of $N/2$, i.e., 0, ±18, ±36,... in this case. Figure 4 shows that only heteronuclear dipolar components with $(m,\mu_S,\mu_K)=(1,-1,-1)$ are symmetry allowed [and by implication, also $(m,\mu_S,\mu_K)=(-1,1,1)$]. The selection of terms with $\mu_S+\mu_K=\pm2$ indicates heteronuclear double-quantum recoupling of the nuclear spin system. Furthermore, the fact that the $(\mu_S,\mu_K)=(-1,-1)$ term is associated with only one spatial rotational component ($m=1$) leads to γ encoding of the recoupled dipolar Hamiltonian. The phase but not the amplitude of the recoupled heteronuclear double-quantum Hamiltonian depends on the Euler angle γ_{MR}.

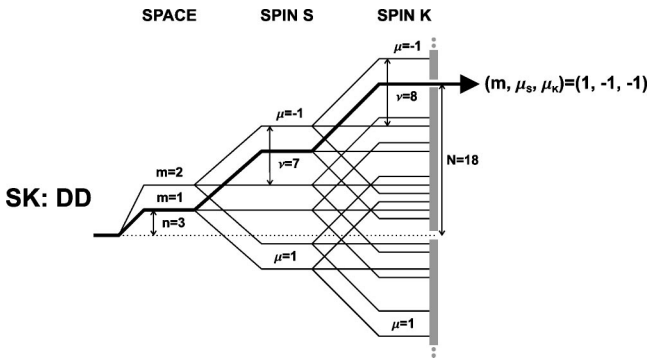

FIG. 4. Space–spin selection diagram for the dual $R18_3^{7,8}$ sequence, continued. Selection of a single heteronuclear double-quantum dipole–dipole component, with quantum numbers $(m,\mu_S,\mu_K)=(1,-1,-1)$. The mirror image pathways stemming from $m=-1$, $m=-2$ have been suppressed for simplicity.

The application of simultaneous C7[11] or POST-C7[13] sequences achieves this type of heteronuclear recoupling, but also recouples the homonuclear dipolar interactions of both spin species S and K.[69]

4. Zero-quantum heteronuclear recoupling

Zero-quantum heteronuclear recoupling sequences provide an average Hamiltonian with the following form:

$$\bar{H}_{SK}^{(1)}=\sum_{s<k}(\omega_{sk}S_s^-K_k^+ + \omega_{sk}^*S_s^+K_k^-). \tag{102}$$

Heteronuclear zero-quantum recoupling as in Eq. (102) may be achieved by changing the sign of either ν_S or ν_K in Tables IV and V. The corresponding μ changes its sign as well. For example, the sequence $R14_3^{2,5}$ recouples the terms $(m,\mu_S,\mu_K)=\{(1,-1,1),(-1,1,-1)\}$, which corresponds to heteronuclear zero-quantum recoupling.

No generalized HH sequences were found that accomplish γ-encoded heteronuclear double- and zero-quantum recoupling at the same time.

The symmetry-allowed terms depend on the relative sense of the rf phase shifts on the S- and K-spins channels. It

TABLE VI. Magnitudes of the scaling factors κ for a selection of $RN_n^{\nu_S,\nu_K}$ and $CRN_n^{\nu_S,\nu_K}$ sequences. The symmetry-allowed terms are shown. m' is the space component of the symmetry allowed term with $(\mu_S,\mu_K)=(-1,-1)$, as used in Eqs. (103) and (110).

Symmetry	(m,μ_S,μ_K)		m'	$\mathscr{R}^S$	$\mathscr{R}^K$	$\lvert\kappa\rvert$
$R22_7^{-6,-9}$	(1,1,1)	(−1,−1,−1)	−1	$90_0270_{90}270_{270}90_0$	$90_0270_{270}270_{90}90_0$	0.221
$R22_7^{9,6}$	(1,−1,−1)	(−1.1,1)	1	$90_{180}360_0180_{180}90_0$	$90_{180}360_0180_{180}90_0$	0.122
$R24_9^{8,7}$	(1,−1,−1)	(−1,1,1)	1	$90_{180}360_0180_{180}90_0$	$90_{180}360_0180_{180}90_0$	0.114
$R24_9^{-5,-10}$	(1,1,1)	(−1,−1,−1)	−1	$60_{180}300_060_{180}$	$60_{180}300_060_{180}$	0.093
Symmetry	(m,μ_S,μ_K)		m'	$\mathscr{C}^S$	$\mathscr{R}^K$	$\lvert\kappa\rvert$
$CR20_7^{-9,-8}$	(1,−1,−1)	(−1,1,1)	1	$90_0360_{180}270_0$	$90_{180}360_0180_{180}90_0$	0.118

is important to take into account the sign of the gyromagnetic ratio γ of the irradiated spin species and the rf mixing scheme on the spectrometer when implementing the sequences shown here.[61,62]

B. Heteronuclear double-quantum recoupling sequences

In the case of γ-encoded heteronuclear double-quantum recoupling, the first order average Hamiltonian is given by Eq. (101). This is provided by generalized HH sequences which recouple the heteronuclear double-quantum terms $(m,\mu_S,\mu_K)=\{(m',-1,-1),(-m',1,1)\}$, where m' is the symmetry-allowed space component, equal to $m'=\pm 1$ depending on the chosen symmetry. The recoupled through-space heteronuclear dipolar interaction depends on the molecular orientation and the starting time point of the dual recoupling sequences t_0^0:

$$\omega_{sk}(\Omega_{MR},t_0^0)=b_{sk}\kappa e^{im'(\omega_r t_0^0-\alpha_{RL}^0-\gamma_{MR})}\times\sum_{m=-2}^{2}d_{0m}^{(2)}(\beta_{PM}^{sk})d_{mm'}^{(2)}(\beta_{MR})\times e^{-im(\gamma_{PM}^{sk}+\alpha_{MR})}, \quad (103)$$

where κ corresponds to scaling factor $\kappa_{2m'1\text{-}11\text{-}1}$ in Eq. (86). The magnitudes of the scaling factors for a selection of pulse sequences are listed in Table VI. The Euler angles $\Omega_{PM}^{sk}=\{\alpha_{PM}^{sk},\beta_{PM}^{sk},\gamma_{PM}^{sk}\}$ describe the transformation of each heteronuclear dipole–dipole coupling from its principal axis system to a molecule fixed frame. The through-space dipolar coupling constant between two spins s and k is given by

$$b_{sk}=-\frac{\mu_0}{4\pi}\frac{\gamma_s\gamma_k\hbar}{r_{sk}^3}, \quad (104)$$

where r_{sk} is the spin–spin internuclear distance.

The scaling factor of the recoupled interaction depends on the choice of the basic elements for the two channels. Generally speaking, it is desirable to choose the basic element so as to maximize the scaling factor κ. At the same it is desirable to choose a sequence which is robust with respect to chemical shift anisotropies, isotropic chemical shifts, and rf amplitude errors. In addition the applied rf fields should be minimized. This is particularly important in systems where the abundant I spins should be decoupled during the recoupling sequence. Normally the rf field on the I spins needs to be a factor of 3 larger than that on the S and K spins to achieve good heteronuclear decoupling,[12,14] although recent studies indicate that this requirement might be weakened at higher MAS spinning frequencies.[70]

In order to identify good candidate sequences we employed a combinatorial approach. We selected a variety of composite pulse elements $\mathscr{E}^0$ which are known to be robust from experience in other fields.[71] For the cyclic element we used $\mathscr{C}=90_0360_{180}270_0$. For the π-rotation elements we considered $\mathscr{R}=90_{315}90_{45}90_{315}$, $90_{180}270_0$, $60_{180}300_060_{180}$, $90_{270}90_090_{90}90_090_{270}90_0$, $90_{90}90_{180}180_{90}90_090_{90}$, 450_0270_{180}, $360_0270_{180}90_0$, $90_{180}360_0180_{180}90_0$, $90_0360_{90}270_{180}$, $90_0270_{90}270_{270}90_0$. In the case of basic elements which are not purely amplitude modulated we also tested the phase-inverted basic element on one channel (see example below). The pulse sequences were tested numerically on an artificial two-spin system including CSA interactions, using all symmetries in Tables IV and V and their derivatives. Sequences passing preliminary tests were examined further under a variety of conditions, including miss-set rf fields. A selection of the most promising sequences were tested experimentally.

The dual sequences $R24_9^{8,7}$ and $R22_7^{9,6}$ with the basic elements $\mathscr{R}^S=\mathscr{R}^K=90_{180}360_0180_{180}90_0$ proved to be relatively robust with respect to rf amplitude errors, isotropic chemical shifts, and chemical shift anisotropies. Experimental results for these sequences are presented below. In simulations, the same symmetries performed well with the basic elements $\mathscr{R}^S=\mathscr{R}^K=360_0270_{180}90_0$. However, the experimental performance of these sequences was slightly worse, for reasons that are unclear.

The sequence $CR20_7^{-9,-8}$ with the basic elements $\mathscr{C}^S=90_0360_{180}270_0$ and $\mathscr{R}^K=90_{180}360_0180_{180}90_0$ or $\mathscr{R}^K=450_0270_{180}$ also performed well in simulations. The choice $\mathscr{R}^K=450_0270_{180}$ was found to perform slightly better experimentally.

The sequence $R22_7^{-6,-9}$ with the basic elements $\mathscr{R}^S=90_0270_{90}270_{270}90_0$ and $\mathscr{R}^K=90_0270_{270}270_{90}90_0$ has a relatively high scaling factor for the recoupled heteronuclear dipolar interactions (see Table VI) but proves rather sensitive with respect to isotropic chemical shifts.

Note the importance of the relative sense of the rf phase shifts on the two channels. For example, the sequence

$R22_7^{-6,-9}$ with basic element $\mathscr{R}^S=\mathscr{R}^K=90_0270_{90}270_{270}90_0$ only has a scaling factor with $|\kappa|=0.046$ and has a much worse performance than the similar sequence with $\mathscr{R}^S=90_0270_{90}270_{270}90_0$ and $\mathscr{R}^K=90_0270_{270}270_{90}90_0$.

In order to facilitate implementation of these pulse sequences, we now give some of them explicitly. The generalized HH sequence $R24_9^{8,7}$ with the basic pulse sequence elements $\mathscr{R}^S=\mathscr{R}^K=90_{180}360_0180_{180}90_0$ is given by

$$S:\ [90_{240}\ \ 360_{60}\ \ 180_{240}\ \ 90_{60}\ \ 90_{120}\ \ 360_{300}\ \ 180_{120}\ \ 90_{300}]^{12}$$
$$K:\ [90_{232.5}\ \ 360_{52.5}\ \ 180_{232.5}\ \ 90_{52.5}\ \ 90_{127.5}\ \ 360_{307.5}\ \ 180_{127.5}\ \ 90_{307.5}]^{12}$$

where the superscript 12 indicates 12 repetitions of the bracketed elements, timed to span a total of nine rotor periods.

The generalized HH sequence $R22_7^{9,6}$ with the basic pulse sequence elements $\mathscr{R}^S=\mathscr{R}^K=90_{180}360_0180_{180}90_0$ is given by

$$S:\ [90_{253.64}\ \ 360_{73.64}\ \ 180_{253.64}\ \ 90_{73.64}\ \ 90_{106.36}\ \ 360_{286.36}\ \ 180_{106.36}\ \ 90_{286.36}]^{11}$$
$$K:\ [90_{229.09}\ \ 360_{49.09}\ \ 180_{229.09}\ \ 90_{49.09}\ \ 90_{130.91}\ \ 360_{310.91}\ \ 180_{130.91}\ \ 90_{310.91}]^{11}$$

where the superscript 11 indicates 11 repetitions of the bracketed elements, timed to span a total of seven rotor periods.

The generalized HH sequence $R22_7^{-6,-9}$ with the basic pulse sequence elements $\mathscr{R}^S=90_0270_{90}270_{270}90_0$ and $\mathscr{R}^K=90_0270_{270}270_{90}90_0$ is given by

$$S:\ [90_{310.91}\ \ 270_{40.91}\ \ 270_{220.91}\ \ 90_{310.91}\ \ 90_{49.09}\ \ 270_{319.09}\ \ 270_{139.09}\ \ 90_{49.09}]^{11}$$
$$K:\ [90_{286.36}\ \ 270_{196.36}\ \ 270_{16.36}\ \ 90_{286.36}\ \ 90_{73.64}\ \ 270_{163.64}\ \ 270_{343.64}\ \ 90_{73.64}]^{11}$$

where the superscript 11 indicates 11 repetitions of the bracketed elements, timed to span a total of seven rotor periods.

V. APPLICATIONS

In this section we demonstrate some different applications of the generalized HH sequences.

A. Heteronuclear correlation spectroscopy

Heteronuclear recoupling sequences may be used to acquire two-dimensional heteronuclear correlation spectra (HETCOR).[72–74] Such spectra correlate the isotropic chemical shifts of coupled heteronuclei. Figure 5 shows an appropriate pulse sequence for this purpose. This is appropriate for two spin species S and K in the presence of abundant spins I with a high gyromagnetic ratio. A common practical case is $I={}^1$H; $S={}^{13}$C; $K={}^{15}$N. The sequence starts with ramped cross polarization to enhance the K-spin magnetization.[38] The transverse magnetization on the K spins is allowed to evolve for an interval t_1 and is then converted into longitudinal magnetization by a $\pi/2$ pulse. A generalized HH sequence is applied to the S and K spins in order to transfer longitudinal magnetization between the spin species. The pulse sequence diagram in Fig. 5 indicates a $RN_n^{\nu_S,\nu_K}$ sequence: In practice, any of the sequences in Tables IV and V might be used. The transferred longitudinal S-spin magnetization is converted to observable magnetization by a $\pi/2$ read pulse and detected in the subsequent period. The time-proportional phase incrementation (TPPI) procedure may be used for obtaining pure-absorption 2D peak shapes.[75] A two-dimensional data matrix $s(t_1,t_2)$ is complied by acquiring a set of transients with incrementation of the interval t_1. The data matrix $s(t_1,t_2)$ is subjected to a complex Fourier transform in the t_2 dimension, and a cosine Fourier transform in the t_1 dimension, in order to obtain the 2D spectrum $S(\omega_1,\omega_2)$.

Figure 6 shows an experimental spectrum obtained with the pulse sequence shown in Fig. 5 on a sample of [98%-U–^{13}C,96%–99%-U–^{15}N]-L-histidine·HCl·H_2O at a field $B_0=9.4$ T and a spinning frequency of $\omega_r/2\pi=14.000$ kHz. The sample was purchased from Cambridge Isotope Laboratories and used without further purification. The experiments were performed on a Chemagnetics Infinity-400 spectrometer using a filled 4 mm zirconia rotor.

The spectrum in Fig. 6(b) was obtained using a cross polarization time of 600 μs. The recoupling was achieved using a $R24_9^{-5,-10}$ sequence, with basic pulse elements given

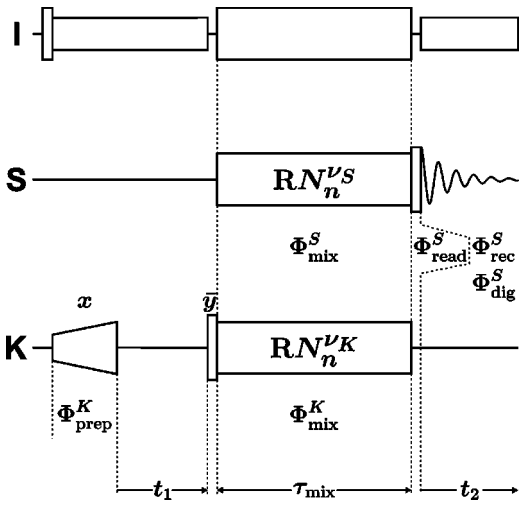

FIG. 5. Radio frequency pulse sequence for two-dimensional heteronuclear correlation spectroscopy between species S and K, in the presence of an abundant species I with high gyromagnetic ratio.

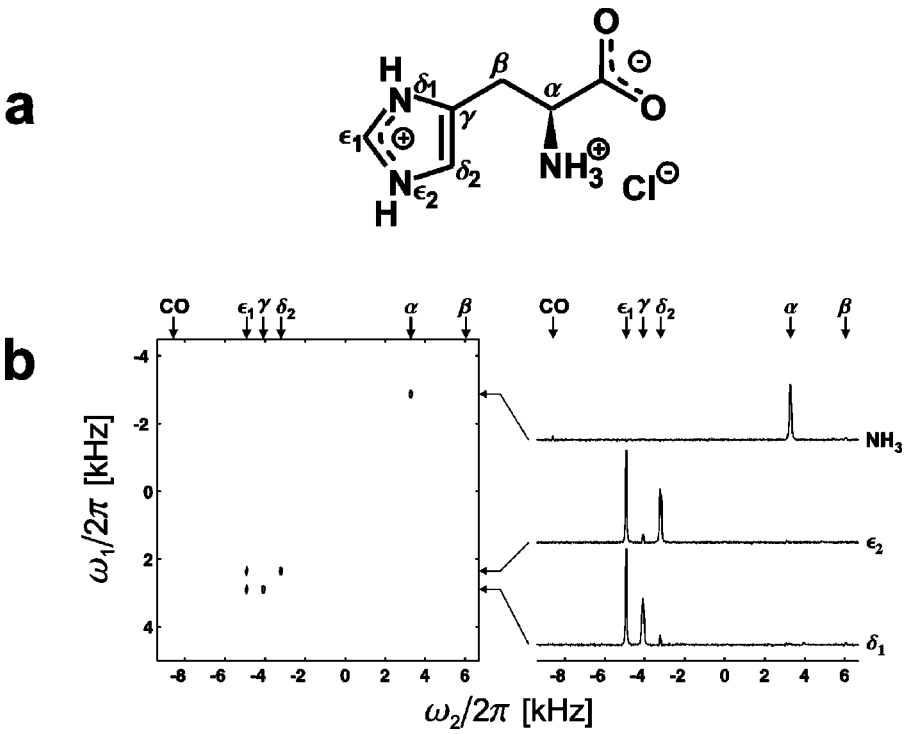

FIG. 6. (a) Molecular structure of L-histidine·HCl. We use the nomenclature recommended by the IUPAC (Ref. 90). (b) Experimental two-dimensional heteronuclear $^{13}C-^{15}N$ correlation spectrum of [98%-U$-^{13}$C,96%$-$99%-U$-^{15}$N]-L-histidine·HCl·H_2O at a field of $B_0=9.4$ T and a spinning frequency of $\omega_r/2\pi=14.000$ kHz, obtained using the pulse sequence in Fig. 5. The recoupling was achieved using a $R24_9^{-5,-10}$ sequence with basic elements $\mathscr{R}^S=\mathscr{R}^K=60_{180}300_060_{180}$. The interval during which the R-sequence irradiation was applied was 1.61 ms. The ω_1 dimension is the ^{13}C single-quantum dimension, whereas the ω_2 dimension is the ^{15}N single-quantum dimension. The assignment of the peaks to the molecular sites is indicated. The sense of the frequency axes respects the signs of the gyromagnetic ratios (Refs. 61 and 62).

by $\mathscr{R}^S=\mathscr{R}^K=60_{180}300_060_{180}$. In total $q_{\mathrm{mix}}=60$ basic elements were used, leading to a total mixing interval of $\tau_{\mathrm{mix}}=1.61$ ms. The evolution interval t_1 was incremented in steps of 5 μs. Continuous-wave proton decoupling was used during the R sequences with a proton nutation frequency of 119 kHz. TPPM decoupling[60] with a proton nutation frequency of 83 kHz was used during the evolution interval t_1 and the data acquisition. The signal in the t_1 dimension was apodized with a $\cos^2$ function and converted into the frequency domain using a cosine transform.

The experimental 2D spectrum in Fig. 5 allows the directly bonded $^{15}N-^{13}C$ connectivities to be traced. The assignment of the ^{13}C and ^{15}N spectra may be completed using a double-quantum ^{13}C spectrum of the same sample, obtained under identical conditions, as shown in Fig. 7. This spectrum was obtained with the modified SC14 pulse sequence[56] described in Appendix C. The two spectra in Figs. 6(b) and 7 may be used to completely assign the ^{13}C and ^{15}N peaks to the molecular sites, without any external knowledge other than the molecular structure. The assignments of the peaks are indicated in the figures.

We have also obtained similar heteronuclear correlation spectra to that shown in Fig. 6(b) using the adiabatic cross-polarization method.[76–78] In principle, the pulse sequences described here should be less susceptible to interference from homonuclear couplings. However, so far we have not been able to demonstrate this advantage decisively.

B. Heteronuclear double-quantum oscillations

Figure 8 shows a rf pulse sequence for passing *S*- and *K*-spin signals through heteronuclear multiple-quantum coherence. The sequence starts with two successive ramped cross-polarization sequences to enhance the *S*- and *K*-spin magnetizations. The following $\pi/2$ pulses on both the *S* and *K* spins convert the cross-polarized transverse magnetizations into longitudinal magnetizations. The ramped cross-polarization field and the $\pi/2$ pulse on the *S*-spin channel

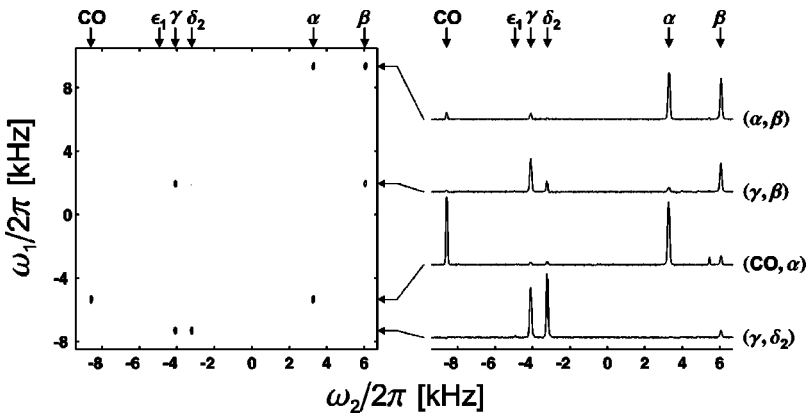

FIG. 7. Experimental two-dimensional homonuclear double-quantum ^{13}C spectrum of [98%-U$-^{13}$C, 96%$-$99%-U$-^{15}$N]-L-histidine·HCl·H_2O at a field of $B_0=9.4$ T and a spinning frequency of $\omega_r/2\pi=14.000$ kHz, obtained using a modified SC14 sequence, as described in Appendix C.

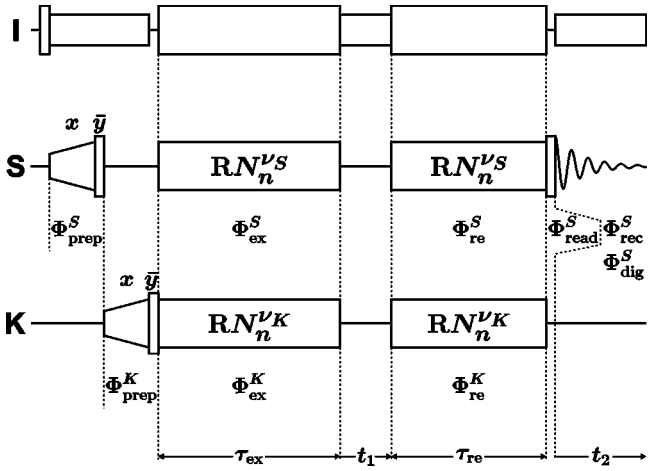

FIG. 8. Radio frequency pulse sequence for passing *S*-spin signals through heteronuclear double-quantum coherence. The phases $\Phi^S_{\rm prep}$, $\Phi^K_{\rm prep}$, $\Phi^S_{\rm ex}$, $\Phi^K_{\rm ex}$, $\Phi^S_{\rm re}$, $\Phi^K_{\rm re}$, and $\Phi^S_{\rm read}$ refer to overall rf phases of the pulse sequence blocks. The rf receiver phase during signal detection is denoted $\Phi^S_{\rm rec}$ and the postdigitization phase by $\Phi^S_{\rm dig}$.

have the phases $\Phi^S_{\rm prep}$ and $\Phi^S_{\rm prep}-\pi/2$, respectively, where $\Phi^S_{\rm prep}$ is the overall rf phase of the preparation interval for the *S* spins. A similar phase $\Phi^K_{\rm prep}$ applies to the *K*-spin preparation.

The heteronuclear double-quantum recoupling sequence of duration $\tau_{\rm ex}$ converts the sum longitudinal magnetization into heteronuclear (± 2)-quantum coherence. The excitation part of the sequence consists of $q_{\rm ex}$ basic elements, where $q_{\rm ex}$ is an even integer. The excitation interval is therefore given by $\tau_{\rm ex}=q_{\rm ex}\tau_E$. The overall phase of the excitation block is denoted $\Phi^S_{\rm ex}$ for the *S* spins and $\Phi^K_{\rm ex}$ for the *K* spins. For the experiments described in this section, there is no interval between the excitation and reconversion pulse sequence, $t_1=0$.

The excited double-quantum coherences are converted into longitudinal magnetization by applying other $q_{\rm re}$ basic elements. The reconversion block has duration $\tau_{\rm re}=q_{\rm re}\tau_E$ and overall phase $\Phi^S_{\rm re}$ for the *S* spins and phase $\Phi^K_{\rm re}$ for the *K* spins. The longitudinal magnetization created by the reconversion sequence is converted into observable magnetization by a $\pi/2$ read pulse, whose phase is denoted $\Phi^S_{\rm read}$.

The complex *S*-spin NMR signal is detected in the subsequent period using a rf receiver phase $\Phi^S_{\rm rec}$ and postdigitization phase shift $\Phi^S_{\rm dig}$.[61]

The pulse sequence phases are cycled in order to select signals passing through heteronuclear double-quantum coherence. The phase-cycles are conveniently specified algebraically using the transient counter $m_t=0,1,2,...$, which is incremented on every acquired transient. The following phase cycles are constructed according to the procedure in Ref. 79.

In the case of isolated $S-K$ spin pairs a relatively short phase cycle may be used since homonuclear multiple-quantum coherence cannot be excited. In this case and if $q_{\rm ex}$ is an even integer, the 16-step phase cycle for dual $RN_n^{\nu_S,\nu_K}$ and $CRN_n^{\nu_S,\nu_K}$ is specified by

$$\begin{aligned}
&\Phi^S_{\rm prep}=\Phi^K_{\rm prep}=\Phi^S_{\rm ex}=\Phi^K_{\rm ex}=0,\\
&\Phi^S_{\rm re}=\frac{\pi}{2}+\frac{\pi}{2}m_t+\Phi^{0,S}_{\rm re},\\
&\Phi^K_{\rm re}=\frac{\pi}{2}+\frac{\pi}{2}m_t,\\
&\Phi^S_{\rm read}=\frac{\pi}{2}+\frac{\pi}{2}m_t+\frac{\pi}{2}\,{\rm floor}\left(\frac{m_t}{4}\right),\\
&\Phi^S_{\rm rec}=0,\\
&\Phi^S_{\rm dig}=\frac{\pi}{2}\,{\rm floor}\left(\frac{m_t}{4}\right)-\frac{\pi}{2}m_t,
\end{aligned} \tag{105}$$

where the function floor(x) returns the largest integer not greater than x.

The phase $\Phi^{0,S}_{\rm re}$ depends on whether a C or a R sequence is used on the *S* spins. For $RN_n^{\nu_S,\nu_K}$, this phase is

$$\Phi^{0,S}_{\rm re}=0. \tag{106}$$

For $CRN_n^{\nu_S,\nu_K}$ sequences, this phase is given by

$$\Phi^{0,S}_{\rm re}=\frac{2\pi\nu_S}{N}q_{\rm ex}. \tag{107}$$

In practice this means that the phase is continuously incremented during the C sequence on the *S* spins under the intervals $\tau_{\rm ex}$ and $\tau_{\rm re}$.

In the case of a multiple *S*- and *K*-spin system, a longer phase cycle is necessary in order to suppress signals passing through homonuclear double-quantum coherences. If $q_{\rm ex}$ is an even integer, the appropriate 32-step phase cycle is specified through

$$\begin{aligned}
&\Phi^S_{\rm prep}=\Phi^K_{\rm prep}=\Phi^S_{\rm ex}=\Phi^K_{\rm ex}=0,\\
&\Phi^S_{\rm re}=\frac{\pi}{2}+\frac{\pi}{2}m_t+\pi\ \ {\rm floor}\left(\frac{m_t}{16}\right)+\Phi^{0,S}_{\rm re},\\
&\Phi^K_{\rm re}=\frac{\pi}{2}+\frac{\pi}{2}m_t,\\
&\Phi^S_{\rm read}=\frac{\pi}{2}+\frac{\pi}{2}m_t+\frac{\pi}{2}\,{\rm floor}\left(\frac{m_t}{4}\right),\\
&\Phi^S_{\rm rec}=0,\\
&\Phi^S_{\rm dig}=\frac{\pi}{2}\,{\rm floor}\left(\frac{m_t}{4}\right)-\pi\ \ {\rm floor}\left(\frac{m_t}{16}\right)-\frac{\pi}{2}m_t,
\end{aligned} \tag{108}$$

where the transient counter takes the values $m_t=0,1,...,31$. The phase $\Phi^{0,S}_{\rm re}$ is specified in Eqs. (106) and (107).

Experimental results for 10% [2-^{13}C,^{15}N]-glycine at $B_0=9.4$ T are shown in Fig. 9. A sample of [2-^{13}C,^{15}N]-glycine was purchased from Cambridge Isotope Laboratories, cocrystallized with natural abundance glycine in a molecular ratio of 1:9 and used without further purification. The experiments were performed on a Chemagnetics Infinity-400 spectrometer using a filled 4 mm zirconia rotor.

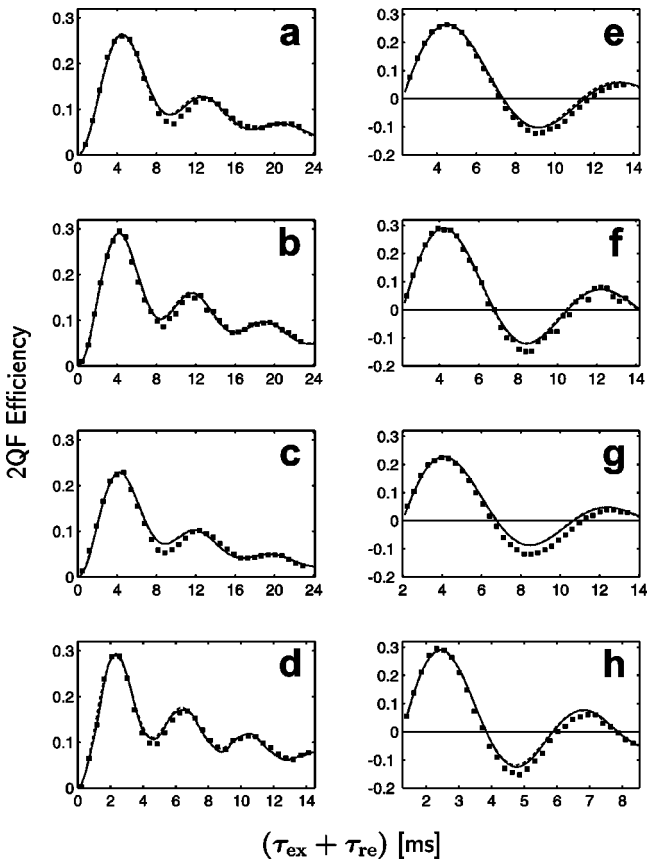

FIG. 9. Symbols: Experimental double-quantum filtered efficiencies obtained on 10% labeled [2-^{13}C,^{15}N]-glycine with the pulse sequence shown in Fig. 8 as a function of $\tau_{ex}+\tau_{re}$. (a)–(d) The excitation and reconversion intervals are incremented simultaneously ($\tau_{ex}=\tau_{re}$). (e)–(h) The excitation interval was fixed, while τ_{re} was varied. (a)–(d) The following symmetries and basic pulse sequence elements were used. (a) and (e): $R24_9^{8,7}$ with $\mathscr{R}^S=\mathscr{R}^K=90_{180}360_0180_{180}90_0$; (b) and (f): $R22_7^{9,6}$ with $\mathscr{R}^S=\mathscr{R}^K=90_{180}360_0180_{180}90_0$; (c) and (g): $CR20_7^{-9,-8}$ with $\mathscr{C}^S=90_0360_{180}270_0$ and $\mathscr{R}^K=450_0270_{180}$; and (d) and (h): $R22_7^{-6,-9}$ with $\mathscr{R}^S=90_0270_{90}270_{270}90_0$ and $\mathscr{R}^K=90_0270_{270}270_{90}90_0$. The following values of τ_{ex} were used: (e) 2.250 ms; (f) 2.212 ms; (g) 1.983 ms; and (h) 1.273 ms. Solid lines: accurate numerical simulations of the amplitudes, multiplied by an exponential function and a vertical scale factor. The following results were obtained for the heteronuclear dipolar coupling constants, the fitted relaxation time constants, and the factors f: (a) and (e): $(b_{SK}/2\pi,T_R,f)=(888\,\text{Hz},14.1\,\text{ms},0.51)$; (b) and (f): $(b_{SK}/2\pi,T_R,f)=(908\,\text{Hz},16.2\,\text{ms},0.52)$; (c) and (g): $(b_{SK}/2\pi,T_R,f)=(904\,\text{Hz},11.6\,\text{ms},0.46)$; and (d) and (h): $(b_{SK}/2\pi,T_R,f)=(916\,\text{Hz},11.9\,\text{ms},0.5)$. Dashed lines: average Hamiltonian simulations ignoring the heteronuclear J coupling, using the same values of the parameters $b_{SK}/2\pi,T,f$ as for the solid line curves. The dashed lines and solid lines are nearly superimposed. Powder averaging was performed using 1154 orientations Ω_{MR}, chosen according to the ZCW scheme (Ref. 91).

Figure 9 shows the experimental heteronuclear double-quantum filtering (2QF) efficiencies for a variety of pulse sequences, plotted as a function of the pulse sequence interval $\tau_{ex}+\tau_{re}$. In all cases the efficiencies were estimated by dividing the ^{13}C peak integrals obtained by the pulse sequence in Fig. 8 by the peak integrals in a simple ramped cross-polarization experiment, using the same number of acquired transients. In the left-hand column of Fig. 9 [plots (a)–(d)], the excitation and reconversion intervals τ_{ex} and τ_{re} were kept equal to each other, both being incremented at the same time (the ''symmetric procedure''). In the right-hand column [plots (e)–(h)], the excitation interval giving the maximum efficiency for the case $\tau_{ex}=\tau_{re}$ was first determined. The excitation interval was fixed to this value while the reconversion interval was incremented, starting at $\tau_{re}=0$. In general, the method in the right column (the ''asymmetric procedure'') provides larger amplitude modulations.[80]

Figures 9(a) and 9(e) illustrate the performance of $R24_9^{8,7}$ with the basic elements $\mathscr{R}^S=\mathscr{R}^K=90_{180}360_0180_{180}90_0$. The results were obtained at a spinning frequency of $\omega_r/2\pi=6.000\,\text{kHz}$, using a cross-polarization contact time of 1.1 ms for ^{13}C and 3 ms for ^{15}N. Continuous wave decoupling was used with the proton nutation frequencies 114 and 81 kHz during the R sequences and acquisition, respectively. The S- and K-spin nutation frequencies during the $R24_9^{8,7}$ sequence were both 32 kHz.

Figures 9(b) and 9(f) were obtained with the sequence $R22_7^{9,6}$, again using the basic elements $\mathscr{R}^S=\mathscr{R}^K=90_{180}360_0180_{180}90_0$. The S- and K-spin nutation frequencies during the $R22_7^{9,6}$ sequence were both 37.7 kHz. The other experimental conditions were the same as in Figs. 9(a) and 9(e). The experimental result clearly shows that this sequence has a slightly larger scaling factor than $R24_9^{8,7}$ (see Table VI).

Figures 9(c) and 9(g) demonstrate the performance of a mixed C/R sequence. In this case the symmetry $CR20_7^{-9,-8}$ was used with the basic elements $\mathscr{C}^S=90_0360_{180}270_0$ and $\mathscr{R}^K=450_0270_{180}$. The S- and K-spin nutation frequencies during the $CR20_7^{-9,-8}$ sequence were both 34.3 kHz. The other experimental conditions were as in Figs. 9(a) and 9(e).

Figures 9(d) and 9(h) illustrate the sequence $R22_7^{-6,-9}$ with the elements $\mathscr{R}^S=90_0270_{90}270_{270}90_0$ and $\mathscr{R}^K=90_0270_{270}270_{90}90_0$. The results were obtained at a spinning frequency of $\omega_r/2\pi=5.500\,\text{kHz}$, using a cross-polarization contact time of 800 μs for ^{13}C and 2.4 ms for ^{15}N. Continuous wave decoupling was used with the proton nutation frequencies 109 and 69 kHz during the R sequences and acquisition, respectively. The S- and K-spin nutation frequencies during the $R22_7^{-6,-9}$ sequence were both 34.6 kHz. The rapid oscillations in these plots confirm that this choice of basic elements provides a large scaling factor for the recoupled heteronuclear interactions, as shown in Table VI.

The solid lines in Fig. 9 are the results of accurate two-spin simulations, using the spin interaction parameters given in Ref. 81. In each case the hetronuclear dipolar coupling constant was varied to obtain the best fit between numerical simulations and experimental results. A multiplicative factor $f\exp\{-(\tau_{ex}+\tau_{re})/T_R\}$ was applied to the numerical simulations to take into account the relaxation during the recoupling sequence and the fact that the cross-polarization procedure does not provide equal S- and K-spin magnetizations. In practice, the fit of the heteronuclear dipolar coupling constant is insensitive to the values of f and the relaxation time constant T_R.

The best fits for the heteronuclear dipolar coupling constants are as follows: (a) and (e) 888 Hz, (b) and (f) 908 Hz, (c) and (g) 904 Hz, and (d) and (h) 916 Hz. In all cases we obtain dipolar coupling constants in the range $902\pm14\,\text{Hz}$. This is in good agreement with the coupling constant of 894

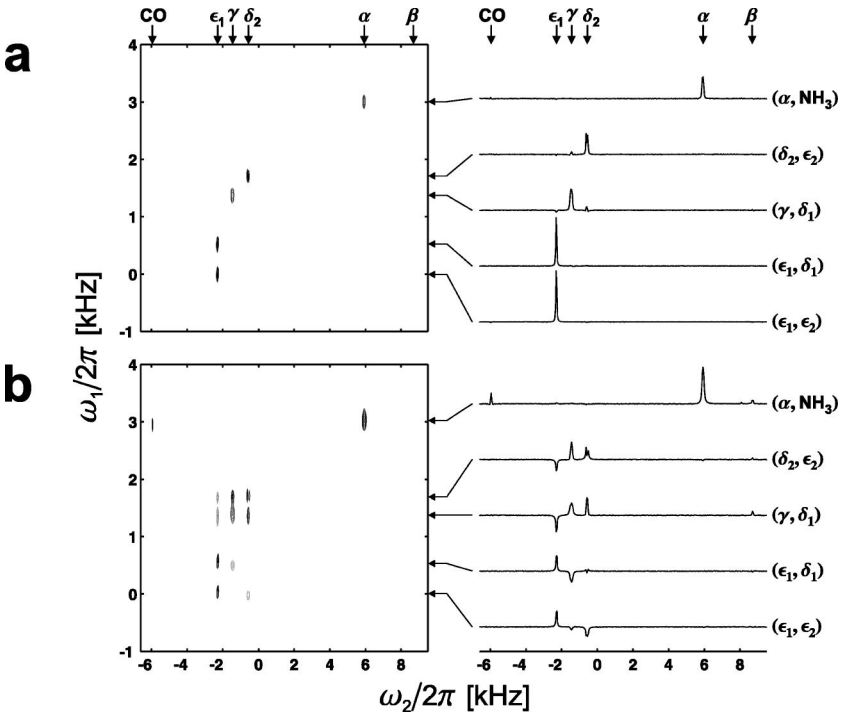

FIG. 10. Experimental two-dimensional heteronuclear double-quantum $^{13}C-^{15}N$ spectra of [98%-U-^{13}C,96%–99%-U-^{15}N]-L-histidine·HCl·H_2O at a field of $B_0=9.4$ T and a spinning frequency of $\omega_r/2\pi=14.000$ kHz, obtained using the pulse sequence in Fig. 8. The recoupling was achieved using a $R24_9^{-5,-10}$ sequence with basic pulse elements $\mathscr{R}^S=\mathscr{R}^K=60_{180}300_060_{180}$. The excitation and reconversion intervals are given by $\tau_{ex}=1232.1\,\mu$s and (a) $\tau_{re}=589.3\,\mu$s and (b) $\tau_{re}=2464.3\,\mu$s. The ω_1 dimension is the ^{13}C single-quantum dimension, whereas the ω_2 dimension is the $^{13}C-^{15}N$ double-quantum dimension.

Hz determined by recent REDOR studies at different sample spinning frequencies.[46] The distance between the C and N nuclei estimated by neutron diffraction is 0.149 nm,[82] which corresponds to a heteronuclear dipolar coupling constant of 926 Hz. The discrepancy between NMR and neutron distance estimations is presumably due to motional averaging of the dipolar coupling constant, as well as J anisotropy.

The dashed lines in Fig. 9 are results of simulations using the average Hamiltonian Eq. (101) with the recoupled heteronuclear dipolar interaction Eq. (103). In all cases the same factor f and exponential decay function were used as for the numerical exact simulations. The average Hamiltonian simulations agree very well with the numerical exact simulations. The good agreement may be attributed to the moderate chemical shift anisotropy of the $^{13}C_\alpha$ site. For larger CSA values one would expect larger deviations.

Further simulations (not shown) indicate that the effect of the heteronuclear isotropic J coupling is negligible.

C. Heteronuclear multiple-quantum spectroscopy

The pulse sequence shown in Fig. 8 may also be used to produce two-dimensional heteronuclear multiple-quantum spectra, in which the frequencies of the heteronuclear (± 2)-quantum coherences are measured in a second frequency dimension. This is done by fixing the intervals τ_{ex} and τ_{re} and by incrementing the interval t_1. The phase cycle must also be adjusted (see below).

Figure 10 shows experimental two-dimensional heteronuclear double-quantum spectra of [98%-U-^{13}C, 96%–99%-U-^{15}N]-L-histidine·HCl·H_2O at $B_0=9.4$ T and a spinning frequency of $\omega_r/2\pi=14.000$ kHz. In both cases, the heteronuclear recoupling was achieved using a $R24_9^{-5,-10}$ sequence, with the basic elements given by $\mathscr{R}^S=\mathscr{R}^K=60_{180}300_060_{180}$. The excitation part of the sequence was the same for the two experiments, and consisted of $q_{ex}=46$ basic elements, corresponding to an excitation interval of $\tau_{ex}=1232.1\,\mu$s.

In Fig. 10(a) the reconversion sequence consisted of $q_{re}=22$ basic elements, corresponding to a reconversion interval of $\tau_{re}=589.3\,\mu$s. In Fig. 10(b) the reconversion sequence consisted of $q_{re}=92$ basic elements, corresponding to a reconversion interval of $\tau_{re}=2464.3\,\mu$s.

These two-dimensional spectra display the frequencies of heteronuclear double-quantum coherences in the ω_1 dimension and the frequencies of single-quantum ^{13}C coherences in the ω_2 dimension. The double-quantum frequencies are equal to the sums of the isotropic chemical shift frequencies of the ^{13}C and ^{15}N nuclei, measured in Hz, taking into account the signs of the gyromagnetic ratios.[61,62] In the present case of $S=^{13}C$ and $K=^{15}N$, the two spin species have opposite signs for their gyromagnetic ratios. In this case the positions of double-quantum peaks in the ω_1 dimension when specified in ppm are given by the *difference* of the chemical shifts of the two spins specified in ppm.

Figure 10(a) shows the two-dimensional heteronuclear double-quantum spectrum for a relatively short reconversion interval ($\tau_{re}=589.3\,\mu$s). In this case, the only peaks of significant amplitude arise from coherence transfer between a double-quantum coherence involving neighboring spins S_j and K_l into a single-quantum coherence of spin S_j, which is a member of the same pair. These have been called *direct* peaks.[56]

In Fig. 10(b) an extended reconversion interval of $\tau_{re}=2464.3\,\mu$s is used. A greater variety of peaks is now observed, some of which are negative. These additional peaks are due to a variety of processes. For example, double quantum coherence may be excited between spins S_j and K_l

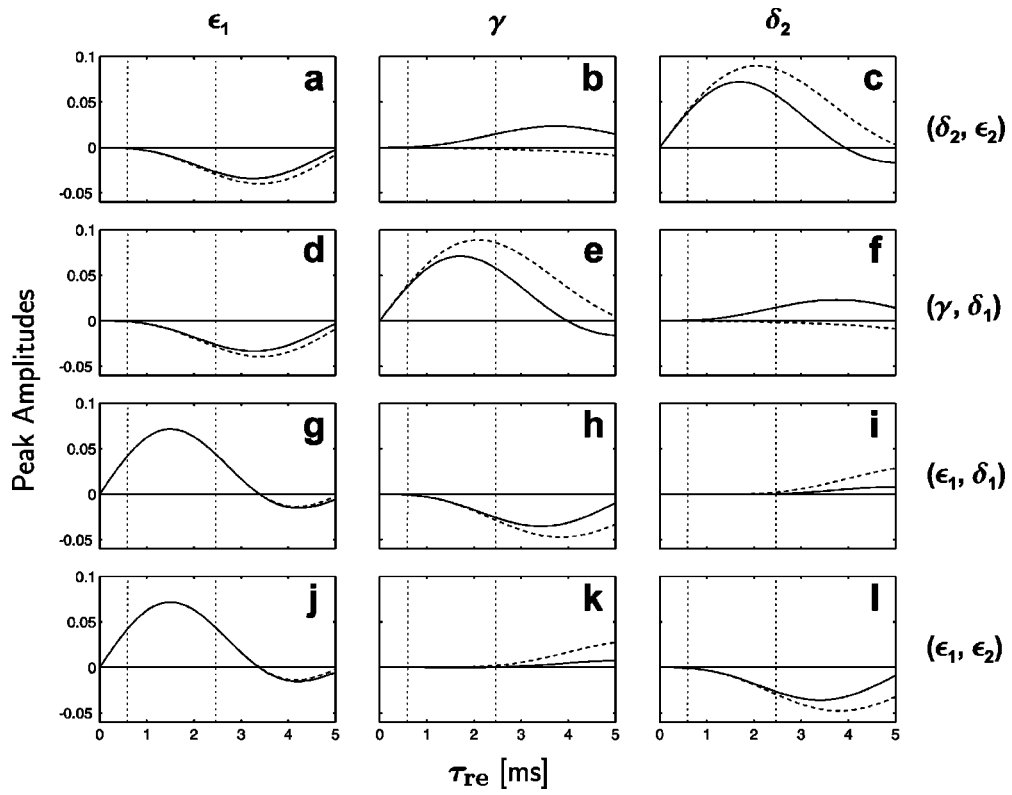

FIG. 11. Average Hamiltonian simulations of the spectral amplitudes of the 12 possible two-dimensional heteronuclear double-quantum spectral peaks of the heteronuclear spin system in the imidazole ring of [98%-U-^{13}C,96%–99%-U-^{15}N]-L-histidine·HCl·H_2O as a function of the reconversion interval τ_{re}. The excitation interval was $\tau_{ex}=1232.1\ \mu$s. The plots show the amplitudes of the spectral peaks corresponding to transfer processes from a heteronuclear double-quantum coherence (S_j,K_l) to a single quantum coherence S_k, denoted $(S_j,K_l)\rightarrow S_k$: (a) $(\delta_2,\epsilon_2)\rightarrow\epsilon_1$; (b) $(\delta_2,\epsilon_2)\rightarrow\gamma$; (c) $(\delta_2,\epsilon_2)\rightarrow\delta_2$; (d) $(\gamma,\delta_1)\rightarrow\epsilon_1$; (e) $(\gamma,\delta_1)\rightarrow\gamma$; (f) $(\gamma,\delta_1)\rightarrow\delta_2$; (g) $(\epsilon_1,\delta_1)\rightarrow\epsilon_1$; (h) $(\epsilon_1,\delta_1)\rightarrow\gamma$; (i) $(\epsilon_1,\delta_1)\rightarrow\delta_2$; (j) $(\epsilon_1,\epsilon_2)\rightarrow\epsilon_1$; (k) $(\epsilon_1,\epsilon_2)\rightarrow\gamma$; and (l) $(\epsilon_1,\epsilon_2)\rightarrow\delta_2$. Solid lines: Simulations using the average Hamiltonian of the recoupled heteronuclear dipolar interactions, Eqs. (101) and (103), as well as a 70 Hz J coupling between the γ and δ_2 carbon sites, Eq. (109). Dashed lines: average Hamiltonian simulations without the $\gamma-\delta_2$ J coupling. Vertical dashed lines indicate the reconversion intervals τ_{re} used in Fig. 10, $\tau_{re}=589.3\ \mu$s and $\tau_{re}=2464.3\ \mu$s. The geometry of the spin system was obtained from Ref. 83. Powder averaging was performed using 1154 orientations Ω_{MR}, chosen according to the ZCW scheme (Ref. 91).

which are not directly bonded but are located some distance away from each other. The extended reconversion interval is able to reconvert these distant double-quantum coherences into single-quantum coherence of spin S_j in the same pair. This is called a *distant direct process*. In addition, the double-quantum coherence between spins S_j and K_l may be converted into single-quantum coherence of a third spin S_k, if the spin S_k also has a heteronuclear coupling to K_l. This transfer is called an *indirect process*. In addition, the heteronuclear coherence between spins S_j and K_l may be converted into single-quantum coherence of a third spin S_k, if S_j and S_k are linked by a network of homonuclear J couplings.

A close examination of the spectrum in Fig. 10(b) indicates multiple origins for the new cross peaks. For example, there are negative cross peaks between the double-quantum coherences of the ^{13}C–^{15}N pair (δ_2,ϵ_2) with the ^{13}C single-quantum coherences of site ϵ_1. This cross peak arises by indirect transfer through the two recoupled heteronuclear spin–spin interactions between δ_2 and ϵ_2 and between ϵ_1 and ϵ_2. Similar processes account for the negative cross peaks between (γ,δ_1) and ϵ_1, between (ϵ_1,δ_1) and γ, and also between (ϵ_1,ϵ_2) and δ_2. Indeed all *possible* indirect cross peaks caused by recoupled heteronuclear interactions between neighboring nuclei appear in Fig. 10(b).

In addition there are strong positive indirect double-quantum peaks between (δ_2,ϵ_2) and γ, and between (γ,δ_1) and δ_2. These peaks are due to homonuclear J couplings (see below).

We examined the spin dynamics in the heteronuclear five-spin system of the imidazole ring by average Hamiltonian simulations. Figure 11 shows the two-dimensional heteronuclear double-quantum peak amplitudes for the 12 possible spectral peaks of the imidazole ring as a function of the reconversion interval τ_{re}. The dashed lines correspond to the case where the average Hamiltonian includes only the recoupled heteronuclear dipolar interactions, Eqs. (101) and (103). The molecular geometry was obtained from Ref. 83. The solid lines correspond to the case where the homonuclear J coupling of around 70 Hz between the γ and δ_2 carbon sites was also included:

$$H_{jk}^{J}=2\pi J_{jk}^{\mathrm{iso}}\mathbf{S}_j\cdot\mathbf{S}_k. \tag{109}$$

This term has the symmetry numbers $(l,m,\lambda_S,\mu_S)=(0,0,0,0)$ and is therefore symmetry allowed under any

CN_n^ν or RN_n^ν sequence. The vertical lines in Fig. 11 indicate the two reconversion intervals τ_{re} for which the experimental two-dimensional spectra are shown in Fig. 10. These simulations show clearly that the homonuclear isotropic J coupling has a considerable effect on the peak amplitudes for larger values of τ_{re}. Figures 11(c), 11(e), 11(g), and 11(j) show the peak amplitudes of the direct peaks observable in Fig. 10(a). Figures 11(a), 11(d), 11(h), and 11(l) show the peak amplitudes for the negative indirect peaks in Fig. 10(b). Figures 11(b) and 11(f) correspond to the positive indirect peaks in Fig. 10(b), which cannot be explained by purely recoupled heteronuclear interactions (dashed lines). If the homonuclear J coupling between the γ and δ_2 carbon site is considered, these simulations explain the occurrence of the positive indirect peaks in Fig. 10(b) (solid lines). The homonuclear J coupling has such a strong effect because it has the same order of magnitude as the scaled recoupled heteronuclear dipolar interaction ($|\kappa b_{SK}| \approx 84$ Hz). The weak positive indirect double-quantum peaks between (α,NH_3) and CO may be attributed to the homonuclear J coupling between the α and CO carbon sites.

Another interesting feature visible in Fig. 10 is that the spectrum of Fig. 10(a) appears to be ''cleaner'' than that in Fig. 6. The ratio of the direct peaks to the indirect peaks is higher in the heteronuclear multiple-quantum spectrum. This effect may be understood using the results for recoupled multiple-spin dynamics presented in Ref. 56. For short reconversion intervals, the amplitudes of the indirect peaks in multiple-quantum filtered spectra are proportional to the cube of the coupling constants multiplied by the reconversion interval, while the amplitudes in conventional correlation spectra are proportional to the first power of the same quantity. It is therefore much easier to suppress long-range peaks and indirect peaks in multiple-quantum and multiple-quantum-filtered spectra. This property should be useful for the spectral methodology of assignment in the solid state NMR of multiply labeled materials.

The spectra shown in Fig. 10 were obtained on a Chemagnetics Infinity-400 spectrometer using a filled 4 mm zirconia rotor. The two spectra were obtained using a cross polarization interval of 2 ms. The evolution interval t_1 was incremented in steps of 25 μs. Continuous-wave proton decoupling was used during the recoupling sequence with a proton nutation frequency of 125 kHz. TPPM decoupling was used during the evolution interval t_1 and the data acquisition with a proton nutation frequency of 101 kHz. The signal in the t_1 dimension was apodized with a $\cos^2$ function and converted into the frequency domain using a cosine transform.

The phase cycle for heteronuclear double-quantum NMR is similar to that given in Eq. (108), but with implementation of the time-proportional phase incrementation (TPPI) procedure used to obtain pure absorption two-dimensional spectra with discrimination of positive and negative ω_1 frequencies.[75] In addition to the transient counter m_t we need the evolution increment counter, denoted m_i, which is incremented between different values of t_1. The transient counter takes the values $m_t = 0,1,...,31$ and the phase specifications are

$$
\begin{aligned}
&\Phi^S_{\mathrm{prep}} = \Phi^K_{\mathrm{prep}} = \Phi^S_{\mathrm{ex}} = \Phi^K_{\mathrm{ex}} = \frac{\pi}{4} m_i ,\\
&\Phi^S_{\mathrm{re}}(t_1) = \frac{\pi}{2} - \frac{1}{2} m' \omega_r t_1 + \frac{\pi}{2} m_t + \pi \ \ \mathrm{floor}\left(\frac{m_t}{16}\right) + \Phi^{0,S}_{\mathrm{re}} ,\\
&\Phi^K_{\mathrm{re}}(t_1) = \frac{\pi}{2} - \frac{1}{2} m' \omega_r t_1 + \frac{\pi}{2} m_t ,\\
&\Phi^S_{\mathrm{read}} = \frac{\pi}{2} + \frac{\pi}{2} m_t + \frac{\pi}{2} \mathrm{floor}\left(\frac{m_t}{4}\right) ,\\
&\Phi^S_{\mathrm{rec}} = 0,\\
&\Phi^S_{\mathrm{dig}} = \frac{\pi}{2} \mathrm{floor}\left(\frac{m_t}{4}\right) - \pi \ \ \mathrm{floor}\left(\frac{m_t}{16}\right) - \frac{\pi}{2} m_t ,
\end{aligned}
\tag{110}
$$

assuming that an even number is chosen for q_{ex}.[84] The phase $\Phi^{0,S}_{re}$ is specified in Eqs. (106) and (107). m' corresponds to that given in Eq. (103) and depends on the chosen symmetry. Table VI specifies m' for the experimental sequences. A two-dimensional data matrix $s(t_1,t_2)$ is compiled by acquiring a set of transients with incrementation of the interval t_1. The data matrix $s(t_1,t_2)$ is subjected to a complex Fourier transform in the t_2 dimension, and a cosine Fourier transform in the t_2 dimension, in order to obtain the 2D spectrum $S(\omega_1,\omega_2)$.

VI. CONCLUSIONS

In this paper we showed that it is technically possible to construct rotor synchronized rf pulse sequences on two radio-frequency channels. The pulse sequence symmetries may be adjusted to obtain selective heteronuclear recoupling between different spin species, while suppressing homonuclear dipole–dipole couplings and chemical shift anisotropies. We showed a number of experimental results, including heteronuclear shift correlation spectroscopy, the estimation of heteronuclear coupling constants, and heteronuclear multiple-quantum NMR.

Where are these generalized HH sequences expected to be useful?

The measurement of distances between spins is unlikely to be a primary area of application. Existing methods such as REDOR[3,4] appear to do a good job, even at long heteronuclear distances. REDOR is also a much simpler pulse sequence and appears to be highly robust. The fact that it is not γ encoded does not appear to be a serious impediment in practice, although it would be desirable to obtain more marked dipolar oscillations, if no other sacrifices were necessary. Nevertheless, the dual rotor-synchronized pulse sequences described here are not expected to compete with REDOR unless homonuclear decoupling is important.

Heteronuclear correlation spectroscopy is also unlikely to benefit much from the sequences presented here. Simpler methods such as adiabatic Hartmann–Hahn cross polarization[76–78] may be a more efficient and reliable way to achieve qualitative magnetization transfer between spin species.

The new pulse sequences may find their main application in heteronuclear multiple-quantum spectroscopy, as

demonstrated in Fig. 10. As mentioned above, heteronuclear multiple-quantum spectra are generally cleaner than single-quantum correlation spectra, providing fewer assignment ambiguities. In addition, the evolution of the heteronuclear multiple-quantum coherence is sensitive to correlated local fields, allowing the estimation of nuclear torsional angles and other angular constraints.[24]

The theorems discussed here may also be applied to other problems, such as the selective recoupling of heteronuclear J interactions[85–87] and the implementation of high-quality heteronuclear decoupling at the same time as homonuclear recoupling. Extension of the two-channel results to three or more channels is also possible. Work in these directions is in progress in our laboratory.

ACKNOWLEDGMENTS

This research was supported by the Göran Gustafson Foundation for Research in the Natural Sciences and Medicine, and the Swedish Natural Science Foundation. One of the authors (A.B.) has been supported by the Marie Curie Research Training Grant ERBFMBICT961439 from the European Union. The authors would like to thank O. G. Johannessen for experimental help and A. Laaksonen for additional computer resources.

APPENDIX A: IMPLEMENTATION OF CN_n^ν AND RN_n^ν SEQUENCES

A. CN_n^ν sequences

Here we prove that the sequence shown in Fig. 1(b) with pulse sequence elements given by Eq. (16) is a CN_n^ν sequence according to the definition in Eq. (14).

The propagators S_q are in this case given by

$$S_q = R_z\left(\frac{2\pi\nu}{N}q\right)S^0 R_z\left(\frac{2\pi\nu}{N}q\right)^\dagger \tag{A1}$$

and

$$E_q = E^0 = R_x(Z_g\pi). \tag{A2}$$

The accumulated propagator up to time point t_q may be written as follows:

$$A_q = S_q E_{q-1}E_{q-2}\cdots E_0 \tag{A3}$$

$$= R_z\left(\frac{2\pi\nu}{N}q\right)S^0 R_z\left(-\frac{2\pi\nu}{N}q\right)R_x(Z_g q\pi). \tag{A4}$$

Since a rotation operator through an even multiple of π is independent of the rotation axis it is valid that $R_x(Z_g q\pi) = R_z(Z_g q\pi)$ and therefore

$$A_q = R_z\left(\frac{2\pi\nu}{N}q\right)S^0 R_z\left(-\frac{2\pi\nu}{N}q\right)R_z(Z_q q\pi). \tag{A5}$$

Since a rotation through an even multiple of π commutes with all other rotations, Eq. (12) may be used to get

$$A_q = R_z\left(\alpha^0 + \frac{2\pi\nu}{N}q + Z_g q\pi\right)R_y(\beta^0)R_z\left(\gamma^0 - \frac{2\pi\nu}{N}q\right). \tag{A6}$$

For CN_n^ν sequences, the first element and the basic element are identical, so we get

$$A_q = R_z\left(\alpha_0 + \frac{2\pi\nu}{N}q + Z_g q\pi\right)R_y(\beta_0)R_z\left(\gamma_0 - \frac{2\pi\nu}{N}q\right). \tag{A7}$$

This proves that the Euler angles β and γ have the symmetry defined in Eq. (14).

B. RN_n^ν sequences

Here we prove that the sequence shown in Fig. 1(c) with pulse sequence elements given by Eq. (20) is a RN_n^ν sequence according to the definition in Eq. (17).

The following relationship between the propagators for the rf field within each element $\mathscr{E}_q$ of the RN_n^ν sequence and the propagator for the rf field within the basic element $\mathscr{R}$ is valid:

$$S_q = R_x(q\pi)R_z\left(\frac{\pi\nu}{N}\right)S^0 R_z\left(\frac{\pi\nu}{N}\right)^\dagger R_x(q\pi)^\dagger. \tag{A8}$$

The propagators E_q are given by

$$E_q = R_x(q\pi)R_z\left(\frac{\pi\nu}{N}\right)R_x(Z_u\pi)R_z\left(\frac{\pi\nu}{N}\right)^\dagger R_x(q\pi)^\dagger. \tag{A9}$$

It is straightforward to prove

$$E_{q-1}E_{q-2}\cdots E_0 = R_x(qZ_u\pi)R_z\left(-\frac{2\pi\nu}{N}q\right). \tag{A10}$$

The accumulated propagator up to time point t_q may be written as follows:

$$A_q = S_q E_{q-1}E_{q-2}\cdots E_0 \tag{A11}$$

$$= R_x(q\pi)R_z\left(\frac{\pi\nu}{N}\right)S^0 R_z\left(-\frac{\pi\nu}{N}\right)$$

$$\times R_x[q(Z_u-1)\pi]R_z\left(-\frac{2\pi\nu}{N}q\right). \tag{A12}$$

Since Z_u-1 is even, the property $R_x[q(Z_u-1)\pi] = R_z[q(Z_u-1)\pi]$ applies. Since a rotation through an even multiple of π commutes with all other rotations, we get

$$A_q = R_x(q\pi)R_z\left(\frac{\pi\nu}{N}+q(Z_u-1)\pi\right)S^0 R_z\left(-\frac{\pi\nu}{N}-\frac{2\pi\nu}{N}q\right)$$

$$= R_x(q\pi)R_z\left(\alpha^0+\frac{\pi\nu}{N}+q(Z_u-1)\pi\right)R_y(\beta^0)$$

$$\times R_z\left(\gamma^0-\frac{\pi\nu}{N}-\frac{2\pi\nu}{N}q\right)$$

$$= R_z\left(-\frac{\pi}{2}\right)R_y(q\pi)R_z\left(\alpha^0+\frac{\pi}{2}+\frac{\pi\nu}{N}+q(Z_u-1)\pi\right)$$

$$\times R_y(\beta^0)R_z\left(\gamma^0-\frac{\pi\nu}{N}-\frac{2\pi\nu}{N}q\right)$$

$$= R_z\left[-\frac{\pi}{2}+(-1)^q\left(\alpha^0+\frac{\pi}{2}+\frac{\pi\nu}{N}\right)+q(Z_u-1)\pi\right]$$

$$\times R_y(\beta^0+q\pi)R_z\left(\gamma^0-\frac{\pi\nu}{N}-\frac{2\pi\nu}{N}q\right) \tag{A13}$$

and hence

$$\beta_q=\beta^0+q\pi,\quad \gamma_q=\gamma^0-\frac{\pi\nu}{N}-\frac{2\pi\nu}{N}q. \tag{A14}$$

This leads to the following values for the Euler angles of the first element

$$\beta_0=\beta^0,\quad \gamma_0=\gamma^0-\frac{\pi\nu}{N} \tag{A15}$$

and hence

$$\beta_q=\beta_0+q\pi,\quad \gamma_q=\gamma_0-\frac{2\pi\nu}{N}q. \tag{A16}$$

This proves that the Euler angles β and γ have the symmetry defined in Eq. (17).

APPENDIX B: GENERAL SCALING FACTORS

A. Single-channel sequences

Assume that the basic element $\mathscr{E}^0$ is built of a sequence of $\mathfrak{N}$ rectangular pulses with flip angles and phases $(\xi_0)_{\phi_0},(\xi_1)_{\phi_1},\ldots,(\xi_{\mathfrak{N}-1})_{\phi_{\mathfrak{N}-1}}$ and rf nutation frequencies $\omega_{\mathrm{nut}}^0,\omega_{\mathrm{nut}}^1,\ldots,\omega_{\mathrm{nut}}^{\mathfrak{N}-1}$. The durations of the pulses are given by $\tau_0,\tau_1,\ldots,\tau_{\mathfrak{N}-1}$, where $\xi_p=\omega_{\mathrm{nut}}^p\tau_p$. Define the pulse Euler angles in the following way:

$$\Omega_p=(A_p,B_p,G_p)=\left(\phi_p-\frac{\pi}{2},-\xi_p,-\phi_p+\frac{\pi}{2}\right). \tag{B1}$$

The factor $K_{m\lambda\mu}$ in Eq. (51) is given by

$$K_{m\lambda\mu}=\sum_{p=0}^{\mathfrak{N}-1}\frac{\tau_p}{\tau_E}\tilde{K}^{(p)}_{m\lambda\mu}, \tag{B2}$$

where the individual pulse contributions $\tilde{K}^{(k)}_{m\lambda\mu}$ are

$$\begin{aligned}
&\tilde{K}^{(0)}_{m\lambda\mu}=K^{(0)}_{m\lambda\mu},\\
&\tilde{K}^{(1)}_{m\lambda\mu}=\exp\{im\omega_\tau\tau_0\}\sum_{\mu'}D^{\lambda}_{\mu\mu'}(\tilde{\Omega}_0)K^{(1)}_{m\lambda\mu'},\\
&\vdots\\
&\tilde{K}^{(p)}_{m\lambda\mu}=\exp\left\{im\omega_r\sum_{p'=0}^{p-1}\tau_{p'}\right\}\sum_{\mu'}D^{\lambda}_{\mu\mu'}(\tilde{\Omega}_{p-1})K^{(p)}_{m\lambda\mu'}.
\end{aligned} \tag{B3}$$

The terms $K^{(p)}_{m\lambda\mu}$ are given by

$$K^{(p)}_{m\lambda\mu}=\exp\{-i\mu A_p\}\tau_p^{-1}\int_0^{\tau_p}dt\,d^{\lambda}_{\mu 0}\left(B_p\frac{t}{\tau_p}\right)\exp\{im\omega_\tau t\}. \tag{B4}$$

The Wigner elements $D^{\lambda}_{\mu\mu'}(\tilde{\Omega}_p)$ are defined through the iteration

$$\begin{aligned}
&D^{\lambda}_{\mu\mu'}(\tilde{\Omega}_p)=\sum_{\mu''}D^{\lambda}_{\mu\mu''}(\tilde{\Omega}_{p-1})D^{\lambda}_{\mu''\mu'}(\Omega_p),\\
&D^{\lambda}_{\mu\mu'}(\tilde{\Omega}_0)=D^{\lambda}_{\mu\mu'}(\Omega_0).
\end{aligned} \tag{B5}$$

If the rf field is modulated smoothly, the scaling factor may be calculated by approximating the modulations as a sequence of small rectangular elements and taking the limit of a large number of steps $\mathfrak{N}$.

B. Dual sequences

The results from the previous section may be generalized for the case of dual sequences. In this case we assume that the basic elements $\mathscr{E}^0_S$ and $\mathscr{E}^0_K$ are divided into a synchronous sequence of $\mathfrak{N}$ rectangular pulses with flip angles and phases $(\xi^S_0)_{\phi^S_0},(\xi^S_1)_{\phi^S_1},\ldots,(\xi^S_{\mathfrak{N}-1})_{\phi^S_{\mathfrak{N}-1}}$ on the S spins and $(\xi^K_0)_{\phi^K_0},(\xi^K_1)_{\phi^K_1},\ldots,(\xi^K_{\mathfrak{N}-1})_{\phi^K_{\mathfrak{N}-1}}$ on the K spins. The durations of the pulses are given by $\tau_0,\tau_1,\ldots,\tau_{\mathfrak{N}-1}$. The nutation frequency of the pulse with index p is $\omega_{\mathrm{nut}}^{S,p}$ and $\omega_{\mathrm{nut}}^{K,p}$ on the S and K spins, respectively, so that $\xi^S_p=\omega_{\mathrm{nut}}^{S,p}\tau_p$ and $\xi^K_p=\omega_{\mathrm{nut}}^{K,p}\tau_p$. If different pulse sequences are used on the S- and K-spin channels, the division between different elements must be simultaneous on the two channels. For example, the choice $\mathscr{E}^0_S=90_{180}270_0$ and $\mathscr{E}^0_K=270_090_{180}$ must be reencoded as $\mathscr{E}^0_S=90_{180}180_090_0$ and $\mathscr{E}^0_K=90_0180_090_{180}$.

Define a set of pulse Euler angles in the following way:

$$\Omega^S_p=(A^S_p,B^S_p,G^S_p)=\left(\phi^S_p-\frac{\pi}{2},-\xi^S_p,-\phi^S_p+\frac{\pi}{2}\right), \tag{B6}$$

$$\Omega^K_p=(A^K_p,B^K_p,G^K_p)=\left(\phi^K_p-\frac{\pi}{2},-\xi^K_p,-\phi^K_p+\frac{\pi}{2}\right). \tag{B7}$$

The factor $K^{SK}_{m\lambda_S\mu_S\lambda_K\mu_K}$ in Eq. (92) is given by

$$K^{SK}_{m\lambda_S\mu_S\lambda_K\mu_K}=\sum_{p=0}^{\mathfrak{N}-1}\frac{\tau_p}{\tau_E}\tilde{K}^{(p)}_{m\lambda_S\mu_S\lambda_K\mu_K}, \tag{B8}$$

where the individual pulse contributions $\tilde{K}^{(p)}_{\lambda_S\mu_S\lambda_K\mu_K}$ are

$$\begin{aligned}
&\tilde{K}^{(0)}_{m\lambda_S\mu_S\lambda_K\mu_K}=K^{(0)}_{m\lambda_S\mu_S\lambda_K\mu_K},\\
&\tilde{K}^{(1)}_{m\lambda_S\mu_S\lambda_K\mu_K}=\exp\{im\omega_r\tau_0\}\sum_{\mu'_S,\mu'_K}D^{\lambda_S}_{\mu_S\mu'_S}(\tilde{\Omega}^S_0)\\
&\qquad\times D^{\lambda_K}_{\mu_K\mu'_K}(\tilde{\Omega}^K_0)K^{(1)}_{m\lambda_S\mu'_S\lambda_K\mu'_K},\\
&\vdots\\
&\tilde{K}^{(p)}_{m\lambda_S\mu_S\lambda_K\mu_K}=\exp\left\{im\omega_r\sum_{p'=0}^{p-1}\tau_{p'}\right\}\sum_{\mu'_S,\mu'_K}D^{\lambda_S}_{\mu_S\mu'_S}(\tilde{\Omega}^S_{p-1})\\
&\qquad\times D^{\lambda_K}_{\mu_K\mu'_K}(\tilde{\Omega}^K_{p-1})K^{(p)}_{m\lambda_S\mu'_S\lambda_K\mu'_K}.
\end{aligned} \tag{B9}$$

The terms $K^{(p)}_{m\lambda_S\mu_S\lambda_K\mu_K}$ are given by

$$K^{(p)}_{m\lambda_S\mu_S\lambda_K\mu_K} = \exp\{-i(\mu_S A^S_p + \mu_K A^S_K)\} \times \tau_p^{-1}\int_0^{\tau_p} dt\, d^{\lambda_S}_{\mu_S 0}\left(B^S_p \frac{t}{\tau_p}\right) d^{\lambda_K}_{\mu K 0}\left(B^K_p \frac{t}{\tau_p}\right) \times \exp\{im\omega_r t\}. \quad \text{(B10)}$$

The Wigner elements $D^{\lambda_S}_{\mu_S\mu_S'}(\tilde{\Omega}^S_p)$ and $D^{\lambda_K}_{\mu_K\mu_K'}(\tilde{\Omega}^K_p)$ are defined through the iterations

$$D^{\lambda_S}_{\mu_S\mu_S'}(\tilde{\Omega}^S_p) = \sum_{\mu_S''} D^{\lambda_S}_{\mu_S\mu_S''}(\tilde{\Omega}^S_{p-1}) D^{\lambda_S}_{\mu_S''\mu_S'}(\Omega^S_p), \quad \text{(B11)}$$

$$D^{\lambda_S}_{\mu_S\mu_S'}(\tilde{\Omega}^S_0) = D^{\lambda_S}_{\mu_S\mu_S'}(\Omega^S_0), \quad \text{(B12)}$$

and

$$D^{\lambda_K}_{\mu_K\mu_K'}(\tilde{\Omega}^K_p) = \sum_{\mu_K''} D^{\lambda_K}_{\mu_K\mu_K''}(\tilde{\Omega}^K_{p-1}) D^{\lambda_K}_{\mu_K''\mu_K'}(\Omega^K_p), \quad \text{(B13)}$$

$$D^{\lambda_K}_{\mu_K\mu_K'}(\tilde{\Omega}^K_0) = D^{\lambda_K}_{\mu_K\mu_K'}(\Omega^K_0). \quad \text{(B14)}$$

The case of smooth rf modulations may be handled by using the limit of large $\mathfrak{N}$.

APPENDIX C: MODIFIED SC14

In this appendix we describe the modified SC14 sequence used to obtain the results shown in Fig. 7. The supercycle is given by

$$\begin{aligned}\mathrm{SC14} = {} & \mathrm{C14}_4^5(0..6)\cdot[\Pi_\pi^{-1}\cdot\mathrm{C14}_4^{-5}(7..13)\cdot\Pi_\pi]_{\pi/7} \\ & \times \mathrm{C14}_4^5(7..13)\cdot[\Pi_0^{-1}\cdot\mathrm{C14}_4^{-5}(0..6)\cdot\Pi_0]_{\pi/7} \\ & \times[\mathrm{C14}_4^5(0..6)]_\pi\cdot[\Pi_\pi^{-1}\cdot\mathrm{C14}_4^{-5}(7..13)\cdot\Pi_\pi]_{8\pi/7} \\ & \times[\mathrm{C14}_4^5(7..13)]_\pi\cdot[\Pi_0^{-1}\cdot\mathrm{C14}_4^{-5}(0..6)\cdot\Pi_0]_{8\pi/7},\end{aligned}$$

where the notation $\mathrm{C14}_4^5(q_1..q_2)$ indicates the use of the elements q_1 to q_2 of the sequence $\mathrm{C14}_4^5$. The notation Π_ϕ indicates the insertion of a π-pulse element with the phase ϕ and Π_ϕ^{-1} indicates the deletion of a π-pulse element. The notation $[\cdots]_\phi$ indicates an overall phase shift of the bracketed sequence by ϕ. The full modified SC14 sequence may be written as follows:

$$\begin{aligned}&360_0\ 360_{128.57}\ 360_{257.14}\ 360_{25.71}\ 360_{154.29}\ 360_{282.86}\ 360_{51.43}\\ &180_{205.71}\ 360_{77.14}\ 360_{308.57}\ 360_{180}\ 360_{51.43}\ 360_{282.86}\ 360_{154.29}\ 180_{205.71}\\ &360_{180}\ 360_{308.57}\ 360_{77.14}\ 360_{205.71}\ 360_{334.29}\ 360_{102.86}\ 360_{231.43}\\ &180_{25.71}\ 360_{257.14}\ 360_{128.57}\ 360_0\ 360_{231.43}\ 360_{102.86}\ 360_{334.29}\ 180_{25.71}\\ &360_{180}\ 360_{308.57}\ 360_{77.14}\ 360_{205.71}\ 360_{334.29}\ 360_{102.86}\ 360_{231.43}\\ &180_{25.71}\ 360_{257.14}\ 360_{128.57}\ 360_0\ 360_{231.43}\ 360_{102.86}\ 360_{334.29}\ 180_{25.71}\\ &360_0\ 360_{128.57}\ 360_{257.14}\ 360_{25.71}\ 360_{154.29}\ 360_{282.86}\ 360_{51.43}\\ &180_{205.71}\ 360_{77.14}\ 360_{308.57}\ 360_{180}\ 360_{51.43}\ 360_{282.86}\ 360_{154.29}\ 180_{205.71},\end{aligned} \quad \text{(C1)}$$

where all flip angles and phases are specified in degrees. The complete sequence spans 16 rotor periods. This version of SC14 was found experimentally to be be slightly more robust with respect to chemical shifts than the version reported in Ref. 56, although this sequence performs slightly worse in numerically exact simulations.

The original SC14 sequence[56] and the modification presented here are conveniently implemented as a sequence of 180° pulses. The 360° pulses are divided into two 180° pulses of the same phase. The total number of 180° pulse elements, used in a recoupling sequence, is called q_{180}, and should be an even integer, even though this means that the sequence might finish after half a 360° pulse. For the original SC14 sequence the best performance is achieved, if q_{180} is a multiple of 28, whereas in the case of the modified SC14 sequence, given in Eq. (C1), q_{180} should be a multiple of 14.

[1] T. G. Oas, R. G. Griffin, and M. H. Levitt, J. Chem. Phys. **89**, 692 (1988).
[2] M. H. Levitt, T. G. Oas, and R. G. Griffin, Isr. J. Chem. **28**, 271 (1988).
[3] T. Gullion and J. Schaefer, J. Magn. Reson. **81**, 196 (1989).
[4] T. Gullion and J. Schaefer, Adv. Magn. Reson. **13**, 57 (1989).
[5] M. H. Levitt, D. P. Raleigh, F. Creuzet, and R. G. Griffin, J. Chem. Phys. **90**, 6347 (1990).
[6] R. Tycko and G. Dabbagh, J. Am. Chem. Soc. **113**, 9444 (1991).
[7] D. M. Gregory, D. J. Mitchell, J. A. Stringer, S. Kiihne, J. C. Shiels, J. Callahan, M. A. Metha, and G. P. Drobny, Chem. Phys. Lett. **246**, 654 (1995).
[8] M. Baldus, M. Tomaselli, B. Meier, and R. R. Ernst, Chem. Phys. Lett. **230**, 329 (1994).
[9] M. Baldus and B. H. Meier, J. Magn. Reson. **128**, 172 (1997).
[10] N. C. Nielsen, H. Bildsøe, H. J. Jakobsen, and M. H. Levitt, J. Chem. Phys. **101**, 1805 (1994).
[11] Y. K. Lee, N. D. Kurur, M. Helmle, O. G. Johannessen, N. C. Nielsen, and M. H. Levitt, Chem. Phys. Lett. **242**, 304 (1995).
[12] C. M. Rienstra, M. E. Hatcher, L. J. Mueller, B. Sun, S. W. Fesik, and R. G. Griffin, J. Am. Chem. Soc. **120**, 10602 (1998).
[13] M. Hohwy, H. J. Jakobsen, M. Edén, M. H. Levitt, and N. C. Nielsen, J. Chem. Phys. **108**, 2686 (1998).
[14] M. Hohwy, C. M. Rienstra, C. P. Jaroniec, and R. G. Griffin, J. Chem. Phys. **110**, 7983 (1999).
[15] M. Helmle, Y. K. Lee, P. J. E. Verdegem, X. Feng, T. Karlsson, J. Lugtenburg, H. J. M. de Groot, and M. H. Levitt, J. Magn. Reson. **140**, 379 (1999).
[16] K. Nomura, K. Takegoshi, T. Terao, K. Uchida, and M. Kainosho, J. Am. Chem. Soc. **121**, 4064 (1999).

[17] M. Carravetta, M. Edén, X. Zhao, A. Brinkmann, and M. H. Levitt, Chem. Phys. Lett. **321**, 205 (2000).
[18] B.-J. van Rossum, C. P. de Groot, V. Ladizhansky, S. Vega, and H. J. M. de Groot, J. Am. Chem. Soc. **122**, 3465 (2000).
[19] V. Ladizhansky and S. Vega, J. Chem. Phys. **112**, 7158 (2000).
[20] Y. Ishii, T. Terao, and M. Kainosho, Chem. Phys. Lett. **265**, 133 (1996).
[21] X. Feng, Y. K. Lee, D. Standström, M. Edén, H. Maisel, A. Sebald, and M. H. Levitt, Chem. Phys. Lett. **257**, 314 (1996).
[22] K. Schmidt-Rohr, J. Am. Chem. Soc. **118**, 7601 (1996).
[23] X. Feng, M. Edén, A. Brinkmann, H. Luthman, L. Eriksson, A. Gräslund, O. N. Antzutkin, and M. H. Levitt, J. Am. Chem. Soc. **119**, 12006 (1997).
[24] M. Hong, J. D. Gross, and R. G. Griffin, J. Phys. Chem. B **101**, 5869 (1997).
[25] P. R. Costa, J. D. Gross, M. Hong, and R. G. Griffin, Chem. Phys. Lett. **280**, 95 (1997).
[26] T. Fujiwara, T. Shimomura, and H. Akutsu, J. Magn. Reson. **124**, 147 (1997).
[27] Y. Ishii, K. Hirao, T. Terao, T. Terauchi, M. Oba, K. Nishiyama, and M. Kainosho, Solid State Nucl. Magn. Reson. **11**, 169 (1998).
[28] M. Hohwy, C. P. Jaroniec, B. Reif, C. M. Rienstra, and R. G. Griffin, J. Am. Chem. Soc. **122**, 3218 (2000).
[29] B. Reif, M. Hohwy, C. P. Jaroniec, C. M. Rienstra, and R. G. Griffin, J. Magn. Reson. **145**, 132 (2000).
[30] S. Ravindranathan, X. Feng, T. Karlsson, G. Widmalm, and M. H. Levitt, J. Am. Chem. Soc. **122**, 1102 (2000).
[31] E. R. Andrew, A. Bradbury, and R. G. Eades, Nature (London) **183**, 1802 (1959).
[32] I. J. Lowe, Phys. Rev. Lett. **2**, 285 (1959).
[33] A. E. Bennett, R. G. Griffin, and S. Vega, NMR **33**, 1 (1994).
[34] S. Dusold and A. Sebald, Annu. Rep. NMR Spectrosc. **41**, 185 (2000).
[35] S. R. Hartmann and E. L. Hahn, Phys. Rev. **128**, 2042 (1962).
[36] A. Pines, M. G. Gibby, and J. S. Waugh, J. Chem. Phys. **59**, 569 (1973).
[37] E. O. Stejskal, J. Schaefer, and J. S. Waugh, J. Magn. Reson. **28**, 105 (1977).
[38] G. Metz, X. Wu, and S. O. Smith, J. Magn. Reson., Ser. A **110**, 219 (1994).
[39] M. Lee and W. I. Goldburg, Phys. Rev. **140**, A1261 (1965).
[40] A. W. Hing, S. Vega, and J. Schaefer, J. Magn. Reson. **96**, 205 (1992).
[41] T. Gullion, Chem. Phys. Lett. **246**, 325 (1995).
[42] T. Gullion, J. Magn. Reson., Ser. A **117**, 326 (1995).
[43] T. Gullion and C. H. Pennington, Chem. Phys. Lett. **290**, 88 (1998).
[44] K. Takegoshi, K. Takeda, and T. Terao, Chem. Phys. Lett. **89**, 331 (1996).
[45] R. Fu, S. A. Smith, and G. Bodenhausen, Chem. Phys. Lett. **272**, 361 (1997).
[46] C. P. Jaroniec, B. A. Tounge, C. M. Rienstra, J. Herzfeld, and R. G. Griffin, J. Magn. Reson. **146**, 132 (2000).
[47] U. Haeberlen and J. S. Waugh, Phys. Rev. **175**, 453 (1968).
[48] J. C. C. Chan, Chem. Phys. Lett. **335**, 289 (2001).
[49] P. Mansfield, M. J. Orchard, D. C. Stalker, and K. H. B. Richards, Phys. Rev. B **7**, 90 (1973).
[50] W. K. Rhim, D. D. Elleman, and R. W. Vaughan, J. Chem. Phys. **59**, 3740 (1973).
[51] D. P. Burum and W. K. Rhim, J. Chem. Phys. **71**, 944 (1979).
[52] D. P. Burum, M. Linder, and R. R. Ernst, J. Magn. Reson. **44**, 173 (1981).
[53] A. Bielecki, A. C. Kolbert, and M. H. Levitt, Chem. Phys. Lett. **155**, 341 (1989).
[54] E. Vinogradov, P. K. Madhu, and S. Vega, Chem. Phys. Lett. **314**, 443 (1999).
[55] M. Edén and M. H. Levitt, J. Chem. Phys. **111**, 1511 (1999).
[56] A. Brinkmann, M. Edén, and M. H. Levitt, J. Chem. Phys. **112**, 8539 (2000).
[57] A. S. D. Heindrichs, H. Geen, C. Giordani, and J. J. Titman, Chem. Phys. Lett. **335**, 89 (2001).
[58] E. H. Hardy, R. Verel, and B. H. Meier, J. Magn. Reson. **148**, 459 (2001).
[59] A. E. Bennett, J. H. Ok, and R. G. Griffin, J. Chem. Phys. **96**, 8624 (1992).
[60] A. E. Bennett, C. M. Rienstra, M. Auger, K. V. Lakshmi, and R. G. Griffin, J. Chem. Phys. **103**, 6951 (1995).
[61] M. H. Levitt, J. Magn. Reson. **126**, 164 (1997).
[62] M. H. Levitt and O. G. Johannessen, J. Magn. Reson. **142**, 190 (2000).
[63] M. H. Levitt, R. Freeman, and T. Frenkiel, Adv. Magn. Reson. **11**, 47 (1983).
[64] D. A. Varshalovich, A. N. Moskalev, and V. K. Khersonskii, *Quantum Theory of Angular Momentum* (World Scientific, Singapore, 1988).
[65] W. Magnus, Commun. Pure Appl. Math. **7**, 649 (1954).
[66] We employ an indexing of the Magnus expansion starting at one. The older literature on average Hamiltonian uses indices which are one less than those given here.
[67] T. Gullion, D. B. Baker, and M. S. Conradi, J. Magn. Reson. **89**, 479 (1990).
[68] X. Zhao, M. Edén, and M. H. Levitt (to be published).
[69] M. Bak, J. T. Rasmussen, and N. C. Nielsen, J. Magn. Reson. **147**, 296 (2000).
[70] A. S. D. Heindrichs, H. Geen, and J. J. Titman, J. Magn. Reson. **147**, 68 (2000).
[71] M. H. Levitt, in *Encyclopedia of Nuclear Magnetic Resonance*, edited by D. M. Grant and R. K. Harris (Wiley, Chichester, England, 1996), Vol. 2, pp. 1396–1411.
[72] P. Caravatti, G. Bodenhausen, and R. R. Ernst, Chem. Phys. Lett. **89**, 363 (1982).
[73] P. Caravatti, L. Braunshweiler, and R. R. Ernst, Chem. Phys. Lett. **100**, 305 (1983).
[74] J. E. Roberts, S. Vega, and R. G. Griffin, J. Am. Chem. Soc. **106**, 2506 (1989).
[75] R. R. Ernst, G. Bodenhausen, and A. Wokaun, *Principles of Nuclear Magnetic Resonance in One and Two Dimensions*, 5th ed. (Clarendon, Oxford, 1988).
[76] S. Hediger, B. H. Meier, N. D. Kurur, G. Bodenhausen, and R. R. Ernst, Chem. Phys. Lett. **223**, 283 (1994).
[77] S. Hediger, B. H. Meier, and R. R. Ernst, Chem. Phys. Lett. **240**, 449 (1995).
[78] M. Baldus, D. G. Geurts, S. Hediger, and B. H. Meier, J. Magn. Reson., Ser. A **118**, 140 (1996).
[79] M. H. Levitt, *Spin Dynamics: Basic Principles of NMR Spectroscopy* (Wiley, Chichester, England, 2001).
[80] M. Carravetta, M. Edén, H. Luthman, P. J. E. Verdegem, J. Lugtenburg, A. Sebald, and M. H. Levitt (to be published).
[81] The following parameters correspond to ''molecule 1'' in Ref. 88 for a ^{13}C Larmor frequency of -100.602 MHz and a ^{15}N Larmor frequency of 40.510 MHz. A molecule-fixed frame M with a z axis along the $^{13}C_{\alpha}-COO$ internuclear vector was chosen. $^{13}C_{\alpha}$ site: isotropic shift $\omega_{\mathrm{iso}}/2\pi=0.0$ Hz, shift anisotropy $\omega_{\mathrm{aniso}}/2\pi=1954.7$ Hz, asymmetry parameter $\eta=0.98$, Euler angles $\Omega_{PM}=\{99.4°,146.0°,138.9°\}$. ^{15}N site: isotropic shift $\omega_{\mathrm{iso}}/2\pi=0.0$ Hz. The CSA of the ^{15}N site was neglected. The internuclear $^{13}C_{\alpha}-^{15}$N vector was oriented at angles $\Omega_{PM}=\{0.0°,112.3°,117.1°\}$. The heteronuclear isotropic J coupling is given by $J_{^{13}C^{15}N}=-6.3$ Hz.
[82] P.-G. Jönsson and Å. Kvick, Acta Crystallogr., Sect. B: Struct. Crystallogr. Cryst. Chem. **28**, 1827 (1972).
[83] H. Fuess, D. Hohlwein, and S. A. Mason, Acta Crystallogr., Sect. B: Struct. Crystallogr. Cryst. Chem. **33**, 654 (1977). The misprinted fractional coordinates for C(1) and H(9) given in this paper are corrected in the Cambridge Structural Database (Ref. 89).
[84] A. Brinkmann, M. Edén, and M. H. Levitt (unpublished).
[85] A. Lesage, S. Steuernagel, and L. Emsley, J. Am. Chem. Soc. **120**, 7095 (1998).
[86] A. Lesage, D. Sakellariou, S. Steuernagel, and L. Emsley, J. Am. Chem. Soc. **120**, 13194 (1998).
[87] A. Lesage, P. Charmont, S. Steuernagel, and L. Emsley, J. Am. Chem. Soc. **122**, 9739 (2000).
[88] R. A. Haberkorn, R. E. Stark, H. van Willigen, and R. G. Griffin, J. Am. Chem. Soc. **103**, 2534 (1981).
[89] F. H. Allen and O. Kennard, Chem. Design Auto. News **8**, 31 (1993).
[90] J. L. Markley, A. Bax, Y. Arata, C. W. Hilbers, R. Kaptein, B. D. Sykes, P. E. Wright, and K. Wüthrich, Pure Appl. Chem. **70**, 117 (1998).
[91] V. B. Cheng, H. H. Suzukawa, and M. Wolfsberg, J. Chem. Phys. **59**, 3992 (1973).
[92] R. K. Hester, J. L. Ackermann, V. R. Cross, and J. S. Waugh, Phys. Rev. Lett. **34**, 993 (1975).